Wavy regime of a colloidal falling film

Darish Jeswin Dhas and Anubhab Roy*
Department of Applied Mechanics, Indian Institute of Technology Madras, Chennai 600036, India

(Received 27 February 2022; accepted 7 June 2022; published 28 June 2022)

In this paper, we study the linear stability and the subsequent formation of nonlinear waves in a colloidal, gravity-driven falling film flow. We first investigate the system's stability by performing a linear stability analysis and observe that the presence of colloidal particles stabilizes both the long-wave surface and the short-wave shear instability modes. The stabilization is attributed to Brownian diffusion equilibrating the leading order particle volume fraction, causing a uniform increase in viscosity. With the particle evolution equation decoupled from the momentum equation in the linear limit, we analytically study the damped yet intricate evolution of perturbations to the particle concentration field. The particle mode decays via three different asymptotic routes: Brownian diffusion, anomalous diffusion, and Taylor dispersion. To study the nonlinear waves, we then derive nonlinear models in the framework of long-wave theory using Benney's gradient expansion approach and the integral-boundary-layer approach. Subsequently, we use a central-manifold approach to derive a depth-averaged equation for the particle volume fraction evolution, incorporating Brownian diffusion and Taylor dispersion. Comparisons of the linear predictions of the nonlinear models with the linear stability calculations show good agreement in the limit of small wave numbers.

DOI: 10.1103/PhysRevFluids.7.064307

I. INTRODUCTION

Falling liquid films are ubiquitous, from water trickling down a windowpane during rainfall to the tear film protecting our eyes. They are observed in diverse engineering and natural scenarios and can occur over a vast range of length and timescales. In industrial processes, the dynamics of falling films play a crucial role in deciding the quality of a coated surface and the heat and/or mass exchange processes across the gas-liquid interface. Falling film dynamics is also an intriguing free-boundary problem that exhibits a prominent wavy regime, often serving as a canonical problem for studying spatiotemporal chaos. Investigations into these wavy dynamics began with the seminal work of Kapitza and Kapitza [1] in 1949 and since then has been extended with further additional physics of electric field [2], thermal effects [3], intermolecular forces [4], topography [5], and surfactants [6] to name a few (also see reviews by Oron *et al.* [7], Craster and Matar [8]). Although several thin-film flows are particle-laden, a falling film's wavy dynamics when the underlying fluid has an evolving microstructure is relatively unexplored. This paper probes the dynamics of a falling film of colloidal suspension, both in the linear and nonlinear regimes.

In the absence of any underlying microstructure, experiments and theoretical investigations on falling film dynamics have shown that waves' inception occurs via long-wavelength disturbances triggering instabilities in an initially uniform laminar flat film—a Nusselt flow [9]. This instability is characterized by the surface waves propagating twice as fast as the mean fluid velocity. Benjamin [10] and Yih [11] predicted the critical Reynolds number for the onset of this instability via a linear stability analysis of the Nusselt flow in the long-wave limit. The subtle effects of unsteady inertia act

*anubhab@iitm.ac.in

as a growth mechanism for these long-wavelength instabilities as they compete with the stabilizing effect of the wall-normal component of gravity [12]. The falling film also exhibits a shear mode instability, similar to other wall-bounded flows [13], with waves propagating slower than the mean fluid velocity and occurring over shorter wavelengths. As observed by Chin *et al.* [14], a distinct difference is that the long-wave surface mode instability has the disturbance amplitude peaking at the free surface; the disturbance amplitude peak occurs closer to the wall in the case of the shear mode instability. They also observed an increase in surface tension and a decrease in inclination angle stabilized the surface mode while destabilizing the shear mode. The shear mode instability occurs at Reynolds numbers that are significantly higher than that of the critical Reynolds number of the long-wave instability, except for very small inclinations [15].

A natural question to ask is what happens to the waves in a falling film when nonlinear effects become important? Benney [16] in 1966 addressed this by performing a long-wave expansion and derived a nonlinear evolution equation for the film height h. The Benney equation correctly predicts the onset of the long-wave instability and its subsequent nonlinear modulations when fluid inertia isn't large. The Benney equation's description of waves in falling films is well studied, including in the framework of dynamical systems [17]. In the small-amplitude limit, the Benney equation reduces to the equation derived by Homsy [18] (also known as the Kuramoto-Sivashinsky equation in literature), a popular reduced-order model for the Navier-Stokes equation for smooth interfaces [9,19]. However, beyond the stability threshold, the Benney equation is susceptible to finite-time blowup [17,20]. The Benney equation's drawback arises from h being the only degree of freedom, thus introducing a high degree of nonlinearity, rendering it unusable for even a modest Reynolds number ($\mathrm{Re} = \rho u_0 h_0/\mu_f$, where ρ is the fluid density, u_0 is the flow velocity, h_0 is the flow length scale, and μ_f is the fluid viscosity). This limitation can be removed using an approach of depth averaging the momentum equation—the integral boundary layer (IBL) approach [21]. This approach involves applying the boundary-layer approximation to the momentum equation and subsequently depth averaging the equation by assuming a self-similar velocity profile alongside the long-wave approximation. A system of two equations is then obtained: an evolution equation for the free surface and an evolution equation for the flow rate. This system no longer faces the finite-time divergence issues that plague the Benney equation.

Recently, several studies have attempted nonlinear modeling of falling films with an additional evolving scalar field in the context of thermocapillary instabilities, with the evolving scalar field being the temperature field inside the film. While investigating thermocapillary instability in falling films, an interfacial instability triggered due to variations in surface tension, Kalliadasis *et al.* [22,23] studied the effects of a local heat source and a uniformly heated bottom plate, respectively. By coupling the momentum and energy equation via the surface tension, which in turn would be a function of temperature, they wrote depth-averaged equations using the IBL approach. Ruyer-Quil *et al.* [24], and Scheid *et al.* [25] later improved the model using an IBL approach but with polynomial test functions for both the velocity and the temperature fields and showed improvements in the predictions of the criticality conditions. They observed that the increase in Prandtl number has a destabilizing effect at small Reynolds numbers and a stabilizing influence at large Reynolds numbers. However, they also observed that their model leads to unphysical negative temperatures in the system for larger Prandtl numbers. Trevelyan *et al.* [26] countered this issue by improving the previous model with modifications to the weight functions.

The dynamics of particle-laden flows can be mapped into a parameter space spanned by three nondimensional numbers: the Reynolds number $\mathrm{Re}_p = \rho_p \dot{\gamma} a^2/\mu_f$ acting as a measure of fluid inertia, the Stokes number $\mathrm{St} = (2/9)a^2\rho_p u_0/\mu_f h_0$ describing the importance of particle inertia, and the Peclet number $\mathrm{Pe}_p = \dot{\gamma} a^2/D_0$ quantifying the role of Brownian motion. Here, ρ_p is the density of the particle, $\dot{\gamma}$ is the shear rate, a is the particle size, $D_0 = k_B T/6\pi\mu_f a$, k_B is the Boltzmann constant, and T is the temperature of the system. For free-surface particle-laden flows, a large body of work exists in the $\mathrm{St} \gg 1$ limit—granular flows [27–30]. Shallow granular flows act as good models for avalanches, mudslides, and pyroclastic flows. The opposite limit, $\mathrm{St} = 0$, is relevant for a wide array of problems in thin films of colloidal suspensions and has received relatively less

attention. The presence of particles influences the fluid rheology, with concentration-dependent viscosity and density being the most obvious changes [31]. Einstein [32] calculated the intrinsic viscosity [$\mathcal{O}(\phi)$] of a dilute suspension of rigid spherical particles. Analyzing the hydrodynamic interaction of a particle pair, Batchelor and Green [33] calculated the next correction [$\mathcal{O}(\phi^2)$] to suspension viscosity. However, these relations are inadequate for high particle concentrations wherein one then uses different empirical models, the Krieger-Dougherty correlation being one of them [34–37]. Also, the particles in the fluid get advected by the motion of the fluid and also diffused either due to thermal effects, as would be in the case of Brownian suspensions [37] or by hydrodynamic effects, as would be the case of non-Brownian suspensions [36,38,39].

Coating processes involve thin films of colloidal suspensions [40–42] and a key requirement in such processes is the deposition of a uniform layer over the substrate, specifically in the paint and inkjet printing industry. Thus it becomes essential to study the stability of shallow layers of colloidal suspension. Several authors have studied drying colloidal thin films using both theoretical and numerical calculations and experiments [42–44]. With the suspended particles being colloidal, implying $\mathrm{Pe}_p \ll 1$, Brownian diffusion dominates in dictating the dynamics of the particles. Goehring *et al.* [45] studied the mechanical instabilities in colloidal film drying using an advection-diffusion equation for the particle phase while accounting for Brownian diffusion and electrostatic contributions to the osmotic pressure with good agreement with experiments. While studying a similar drying process, Wang and Brady [46] performed calculations using both a simple advection-diffusion equation accounting only for Brownian diffusion and compared the results with Brownian dynamics (BD) simulations. They show that the model agrees well with the BD simulations as long as $\mathrm{Pe}_p \ll 1$. Sobac *et al.* [47] predicted the onset of the Benard-Marangoni instability using a similar advection-diffusion equation with good agreement with experiments. In the context of freezing colloidal suspensions, Peppin *et al.* [48] performed a linear stability analysis using a similar formulation and identified a mechanism for pattern formations. Nevertheless, what is left unexplored is the interfacial stability and wavy dynamics of a gravity-driven colloidal film.

In the problem of a thin film with a moving contact line with negatively buoyant non-Brownian suspensions, Zhou *et al.* [49] used the lubrication approximation and balance of viscous and gravitational forces to arrive at a coupled set of equations. However, they assumed the concentration constant along the gradient direction, not allowing particles to settle. Cook [38] extended the model to include the effect of particle settling by a balance of settling to shear-induced migration using the diffusive flux approach. Murisic *et al.* [36,39] extended the model developed by Cook [38] to study the well-mixed and settled regimes of the particles in the film. Mavromoustaki *et al.* [50] extended the work of Murisic *et al.* [36] with the inclusion of the surface tension terms. They observed that the inclusion of surface tension terms helped regularize the film height by suppressing the unphysical singular shock that is known to occur in its absence. To study the accumulation of non-Brownian particles in the advancing meniscus leading to a viscous fingering instability, Chen *et al.* [51] derived a depth-averaged particle concentration equation showing a self-similar behavior of the particles. In the case of Brownian suspensions, Espin and Kumar [37] studied the spreading of thin films and droplets with colloidal suspensions using a similar lubrication theory-based formalism. In the absence of shear-induced migration and gravitational fluxes, the particle concentration is uniform in the wall-normal direction at leading order (diffusion is the sole agent in the gradient direction and acts rapidly to equilibrate the concentration field). Pham and Kumar [52] used a similar formulation for the problem of an evaporating drop with colloidal suspensions on a permeable substrate. They showed that evaporation and imbibition tend to have the same effect in promoting an increase in the particles' concentration toward the droplet's contact line.

This paper focuses on studying the interfacial stability of a gravity-driven falling colloidal liquid film, starting from a linear stability analysis to a long-wave nonlinear analysis. In the present paper, we will be studying Brownian suspensions, ignoring the effects of shear-induced migration and particle-induced normal stresses. Our goal is twofold: analyze particle concentration field evolution in a Nusselt flow and then derive a consistent reduced-order model for describing particle transport in falling films. If we exclude fluid inertia ($\mathrm{Re} = \rho u_0 h_0/\mu_f = 0$), velocity disturbances on a falling

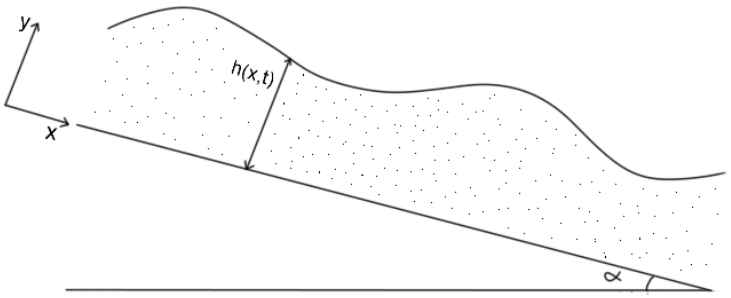

FIG. 1. Schematic of a colloidal falling film.

film will manifest as traveling damped waves, entirely along expected lines. Even in this seemingly uninteresting regime, the particle concentration field ϕ displays vibrant dynamics. We conduct a linear stability analysis to find an analytical solution for particle concentration perturbations, labeled as a particle mode. As expected, it is a purely damped mode but has three asymptotics limits for the decay rate: a pure Brownian mode ($\sim k^2/\mathrm{Pe}$), a Taylor mode ($\sim k^2\mathrm{Pe}$), and an anomalous mode ($\sim\sqrt{k/\mathrm{Pe}}$). Here k is the streamwise wave number and $\mathrm{Pe} = u_0 h/D_0$ is the Peclet number defined based on film thickness (h_0). The insights from the linear stability analysis are crucial in formulating the nonlinear wave models. Using central manifold analysis [53], we derive a nonlinear evolution equation for $\phi(x,t)$ that captures the physics of Taylor dispersion. Next, we incorporate fluid inertia effects and derive a Benney-like equation and IBL equations describing a particle-laden falling film's wavy regime. As discussed earlier in the context of heated falling films, coupling the evolution of an additional scalar field to the IBL equations is nontrivial. Since the typical Grashof number for heated falling films is small, most studies ignore the buoyancy forcing in the momentum equations; the coupling occurs only at the interfacial boundary conditions [9]. Particle-laden falling films, with concentration-dependent viscosity, do not offer us such comfort. We study the derived reduced-order models using numerical simulations and analyze the modification of nonlinear waves by particle concentration.

The organization of the paper is as follows. Section II describes the problem to be studied. Section III deals with the system's linear stability analysis, looking into the surface mode, shear mode, and particle mode. To probe the nonlinear regime, a model based on the asymptotic expansion approach of Benney [16] is derived in Sec. IV with a center manifold approach used to incorporate Taylor dispersion for the particle phase. The nonlinear waves after the onset of instability are studied in Sec. IV A. With the shortcomings of the modified Benney equations, a boundary layer approximation-based approach is then used to derive the IBL model for the coupled system that accommodates small to moderate Reynolds numbers in Sec. IV B. Finally, we discuss the linear stability analysis and the nonlinear models in Sec. V and summarize the work in Sec. VI.

II. PROBLEM FORMULATION

We will consider a particle-laden two-dimensional viscous incompressible thin film falling down an inclined plane under the action of gravity (see Fig. 1). The particles are colloidal, neutrally buoyant, and are assumed to be rigid. Therefore, we assume that the Reynolds number (Re_p) and Peclet number (Pe_p) associated with the particle size are vanishingly small. The substrate is inclined at an angle α, and the instantaneous height of the film is taken as $h(x,t)$. With the presence of particles, the effective viscosity becomes a function of the particle volume fraction (ϕ) and is written as $\mu(\phi)$. The governing equations for this system are

$$\boldsymbol{\nabla}\cdot\boldsymbol{u} = 0, \tag{1}$$

$$\rho\left(\frac{\partial \boldsymbol{u}}{\partial t} + \boldsymbol{u}\cdot\boldsymbol{\nabla}\boldsymbol{u}\right) = \boldsymbol{\nabla}\cdot\boldsymbol{T} + \rho\boldsymbol{g}, \tag{2}$$

where $\mathbf{u} = (u, v)$ is the velocity field, ρ the density, and $\boldsymbol{T}$ is the stress tensor denoted as

$$\boldsymbol{T} = -P\boldsymbol{I} + \mu(\phi)(\nabla \boldsymbol{u} + \nabla \boldsymbol{u}^T). \tag{3}$$

P is the pressure field and $\boldsymbol{I}$ the identity tensor. In the above system, the particle contribution enters only through the modification of shear stresses, ignoring the particle normal stresses' contribution. Since the problem focuses on capturing the colloidal particles' effects and normal stresses scale as particle size squared [54], this simplification holds. We complement the above equations with the following boundary conditions:

(1) The no-slip, no-penetration boundary conditions at $y = 0$:

$$\boldsymbol{u} = 0. \tag{4}$$

(2) The balance of normal and tangential stresses at the free interface $y = h(x, t)$,

$$P = \frac{2\mu(\phi)}{1 + \left(\frac{\partial h}{\partial x}\right)^2}\left[\left(\frac{\partial h}{\partial x}\right)^2 \frac{\partial u}{\partial x} - \frac{\partial u}{\partial y}\frac{\partial h}{\partial x} - \frac{\partial v}{\partial x}\frac{\partial h}{\partial x} + \frac{\partial v}{\partial y}\right] - \frac{\sigma \frac{\partial^2 h}{\partial x^2}}{\left[1 + \left(\frac{\partial h}{\partial x}\right)^2\right]^{3/2}}, \tag{5}$$

$$0 = 4\mu(\phi)\frac{\partial u}{\partial x}\frac{\partial h}{\partial x} - \mu(\phi)\left(1 - \left(\frac{\partial h}{\partial x}\right)^2\right)\left(\frac{\partial u}{\partial y} + \frac{\partial v}{\partial x}\right), \tag{6}$$

where σ is the surface tension. Marangoni forces due to the inhomogeneity in interfacial particle concentration are ignored here.

(3) The kinematic boundary condition at the free interface $y = h(x, t)$:

$$\frac{\partial h}{\partial t} + u\frac{\partial h}{\partial x} = v. \tag{7}$$

The concentration-dependent viscosity is obtained from the Krieger-Dougherty correlation [37] as

$$\mu = \mu_f\left(1 - \frac{\phi}{0.64}\right)^{-2} = \mu_f \kappa(\phi), \tag{8}$$

where μ_f denotes the fluid viscosity. For convenience, the nondimensional part of viscosity is written as $\kappa(\phi)$. As can be noted, the viscosity diverges at a volume fraction of 0.64, which for hard spheres is the maximum random packing fraction. The evolution of the particle concentration is described by an advection-diffusion equation for the volume fraction of the particles ϕ,

$$\frac{\partial \phi}{\partial t} + \boldsymbol{u} \cdot \nabla\phi = \nabla(\boldsymbol{D} \cdot \nabla\phi), \tag{9}$$

where $\boldsymbol{D}$ is the diffusion tensor. Here the effects of shear-induced migration on the particle flux are neglected. This is because, in the case of colloidal particles, Brownian diffusion can be seen to be dominant. For near-equilibrium colloidal dispersions, the diffusion tensor is isotropic ($\boldsymbol{D} = D\boldsymbol{I}$) and is given by the generalized Stokes-Einstein relation [31],

$$\begin{aligned} D &= D_0 \mathcal{K}(\phi)\frac{d}{d\phi}[\phi Z(\phi)], \\ &= D_0(1-\phi)^{6.55}\frac{d}{d\phi}\left(\frac{1.85\phi}{0.64-\phi}\right), \\ &= D_0(1-\phi)^{6.55}\frac{1.184}{(0.64-\phi)^2}, \end{aligned} \tag{10}$$

where $D_0 = k_B T/6\pi\mu_f a$ is the free particle diffusion coefficient with k_B being the Boltzmann constant, T being the characteristic temperature, and a being the particle radius. In Eqs. (10), $\mathcal{K}(\phi)$ denotes the sedimentation coefficient for which the Richardson-Zaki correlation for the

sedimentation coefficient is used and $Z(\phi)$ is the compressibility factor adopted from Espin and Kumar [37]. Similar to the way viscosity is written, the nondimensional part of diffusivity is written as $\Upsilon(\phi)$ such that $D = D_0\Upsilon(\phi)$. Equation (9) is complemented by the no-flux boundary condition at solid substrate $y = 0$,

$$\frac{\partial \phi}{\partial y} = 0, \tag{11}$$

and the same at the free surface $y = h(x, t)$:

$$-D\left[\frac{\partial \phi}{\partial y} - \frac{\partial h}{\partial x}\frac{\partial \phi}{\partial x}\right] = 0. \tag{12}$$

The governing equations are rendered dimensionless with the film height (h_0) for length scales, the velocity of a falling film devoid of particles ($u_0 = \rho g h_0^2 \sin\alpha/3\mu_f$) for the velocity scale, and an inertial scale for pressure. With the Reynolds number as $\mathrm{Re} = \rho h_0 u_0/\mu_f$, the Peclet number as $\mathrm{Pe} = u_0 h_0/D_0$, and the Weber number as $\mathrm{We} = \sigma/(\rho u_0^2 h_0)$, the nondimensional equations are written as

$$\frac{\partial u}{\partial x} + \frac{\partial v}{\partial y} = 0, \tag{13}$$

$$\mathrm{Re}\left(\frac{\partial u}{\partial t} + u\frac{\partial u}{\partial x} + v\frac{\partial u}{\partial y}\right) = -\mathrm{Re}\frac{\partial P}{\partial x} + \frac{\partial}{\partial x}\left(\kappa(\phi)\frac{\partial u}{\partial x}\right) + \frac{\partial}{\partial y}\left(\kappa(\phi)\frac{\partial u}{\partial y}\right) + \frac{\partial \kappa(\phi)}{\partial y}\frac{\partial v}{\partial x} - \frac{\partial \kappa(\phi)}{\partial x}\frac{\partial v}{\partial y} + 3, \tag{14}$$

$$\mathrm{Re}\left(\frac{\partial v}{\partial t} + u\frac{\partial v}{\partial x} + v\frac{\partial v}{\partial y}\right) = -\mathrm{Re}\frac{\partial P}{\partial y} + \frac{\partial}{\partial x}\left(\kappa(\phi)\frac{\partial v}{\partial x}\right) + \frac{\partial}{\partial y}\left(\kappa(\phi)\frac{\partial v}{\partial y}\right) + \frac{\partial \kappa(\phi)}{\partial x}\frac{\partial u}{\partial y} - \frac{\partial \kappa(\phi)}{\partial y}\frac{\partial u}{\partial x} - 3\cot\alpha, \tag{15}$$

$$\mathrm{Pe}\left(\frac{\partial \phi}{\partial t} + u\frac{\partial \phi}{\partial x} + v\frac{\partial \phi}{\partial y}\right) = \frac{\partial}{\partial x}\left(\Upsilon(\phi)\frac{\partial \phi}{\partial x}\right) + \frac{\partial}{\partial y}\left(\Upsilon(\phi)\frac{\partial \phi}{\partial y}\right). \tag{16}$$

The boundary conditions at $y = 0$ are

$$u = v = 0, \quad \frac{\partial \phi}{\partial y} = 0, \tag{17}$$

and at $y = h$ are

$$\mathrm{Re}\ P = \frac{2\kappa(\phi)}{\left[1 + \left(\frac{\partial h}{\partial x}\right)^2\right]}\left[\left(\frac{\partial u}{\partial x}\left(\frac{\partial h}{\partial x}\right)^2 - \frac{\partial v}{\partial x}\frac{\partial h}{\partial x}\right) - \frac{\partial u}{\partial y}\frac{\partial h}{\partial x} + \frac{\partial v}{\partial y}\right] - \frac{\mathrm{We}\ \mathrm{Re}\ \frac{\partial^2 h}{\partial x^2}}{\left[1 + \left(\frac{\partial h}{\partial x}\right)^2\right]^{3/2}},$$

$$0 = 4\kappa(\phi)\frac{\partial u}{\partial x}\frac{\partial h}{\partial x} - \kappa(\phi)\left(1 - \left(\frac{\partial h}{\partial x}\right)^2\right)\left(\frac{\partial u}{\partial y} + \frac{\partial v}{\partial x}\right),$$

$$\Upsilon(\phi)\frac{\partial h}{\partial x}\frac{\partial \phi}{\partial x} - \Upsilon(\phi)\frac{\partial \phi}{\partial y} = 0, \quad \frac{\partial h}{\partial t} + u\frac{\partial h}{\partial x} = v. \tag{18}$$

For the sake of brevity, we use the same notation for the nondimensional quantities. It must be noted that since we are considering the particles to be colloidal, the Reynolds number (Re) and

Peclet number (Pe) based on the film thickness are taken to be finite, whereas, the Reynolds number (Re_p) and Peclet number (Pe_p) based on the particle size are negligible.

III. LINEAR STABILITY ANALYSIS

For the linear stability analysis, the solution of a steady, unidirectional flow is taken as the base state, which is a constant particle concentration ϕ_b and a half -parabolic Nusselt flow given by

$$u_b = 3\kappa_b^{-1}\left(y - \frac{y^2}{2}\right), \tag{19}$$

where $\kappa_b = (1 - \phi_b/0.64)^{-2}$. A normal mode analysis is done by perturbing the variables in the problem as a sum of their base states and a sinusoidal wave of wave number k and wave speed c, with a said infinitesimally small amplitude. Thus, each physical parameter in the system (say X) are written in the form $X = X_b + \hat{X}\, e^{ik(x-ct)}$, with X_b referring to the base flow variables and $\hat{X}$ referring to the infinitesimally small amplitude of the disturbances. This linearization of the momentum and particle concentration equations [Eqs. (13)–(16)] give a system of linear equations

$$\left\{ik\mathrm{Re}\left[(u_b - c)(\mathcal{D}^2 - k^2) - u_b''\right] - \kappa_b(\mathcal{D}^2 - k^2)^2\right\}\hat{\psi} = \kappa_{b1}(\mathcal{D}^2 + k^2)(u_b'\hat{\phi}), \tag{20}$$

$$\{\Upsilon_b(\mathcal{D}^2 - k^2) - ik\mathrm{Pe}(u_b - c)\}\hat{\phi} = 0, \tag{21}$$

where $\hat{\psi}$ and $\hat{\phi}$ are perturbation stream function and concentration field, respectively, $\mathcal{D}$ and primes denote the derivatives with respect to y of the perturbation and base state quantities, respectively. $\kappa_{b1} = d\kappa_b/d\phi_b$ is a consequence of expansion of the viscosity term. The linearized boundary conditions can be subsequently written at $y = 1$ as

$$\left\{\kappa_b\left(\mathcal{D}^2 + k^2\right) - \frac{3}{(c - u_b(1))}\right\}\hat{\psi} = 0, \tag{22}$$

$$\left\{\kappa_b\left(\mathcal{D}^2 - 3k^2\right)\mathcal{D} + ik\mathrm{Re}(c - u_b(1))\mathcal{D} - (3\cot\theta + k^2\ \mathrm{We}\ \mathrm{Re})\frac{ik}{(c - u_b(1))}\right\}\hat{\psi}$$
$$+ \kappa_{b1}\mathcal{D}\left(u_b'\hat{\phi}\right) = 0, \tag{23}$$

$$-\Upsilon_b\, \mathcal{D}\hat{\phi} = 0 \tag{24}$$

and at $y = 0$:

$$\hat{\psi} = 0, \quad \mathcal{D}\hat{\psi} = 0, \quad \mathcal{D}\hat{\phi} = 0. \tag{25}$$

The above set of equations reveal an interesting feature: $\hat{\phi} = 0$ is a solution of the above system with the subsequent equations becoming similar to that of Yih [11] but with a modified viscosity.

A. Particle mode

Since the particle perturbation equation is decoupled from the momentum perturbation equation, it essentially becomes a particle concentration field evolving on top of a background Nusselt flow. For a Nusselt flow, Eq. (21) that arises from the $\hat{\phi}$ evolution can be written in a more compact form

$$\mathcal{D}^2\hat{\phi} = \frac{1}{\xi}\left\{\lambda + iy\left(1 - \frac{y}{2}\right)\right\}\hat{\phi}, \tag{26}$$

where

$$\xi = \frac{\Upsilon_b\kappa_b}{3k\mathrm{Pe}}, \tag{27}$$

$$\lambda = -\frac{1}{3}ic\kappa_b + k^2\xi. \tag{28}$$

The above equation admits an analytic solution in terms of Hermite functions as

$$\hat{\phi} = e^{-z^2/2}\{C_1\mathcal{H}_n(z) + C_2\mathcal{H}_n(-z)\}, \tag{29}$$

where

$$z = (2\xi)^{-1/4}e^{-i\pi/8}(y-1), \tag{30}$$

$$n = -\frac{1}{2} - \frac{1}{\sqrt{2\xi}}\left(\lambda + \frac{i}{2}\right)e^{i\pi/4}. \tag{31}$$

Previous studies on advection-diffusion equations, similar to Eq. (21), have shown that the evolution of a passive scalar is governed by two distinct timescales, separating three regimes of dispersive (diffusive) behavior: Brownian diffusion, anomalous diffusion, and Taylor dispersion [55,56]. Here, Taylor dispersion refers to the enhanced dispersion that occurs along the flow direction under the combined action of molecular diffusion and shear [57]. Anomalous diffusion, on the other hand, refers to the intermediary regime that is neither Brownian diffusion nor Taylor dispersion. These transitions are a consequence of the competition between the asymptotic limits of the Peclet numbers and the film aspect ratio (ϵ) [56]. Brownian diffusion would dominate for $\mathrm{Pe} \ll 1$, with a timescale of $\mathcal{O}(\mathrm{Pe})$. The presence of anomalous diffusion is characterized by a timescale $\sqrt{\mathrm{Pe}}$ smaller than the Brownian diffusion. At the same time, Taylor dispersion is associated with a timescale Pe^2 smaller than Brownian diffusion. Thus anomalous diffusion and Taylor dispersion become relevant only in cases where the relevant Peclet number is large [58]. We will now explore the transition between the three regimes, guided by the approach of Camassa *et al.* [56]. First, the limit of $\xi \to \infty$, which in turn implies that $k\mathrm{Pe} \to 0$ is studied. Solving Eq. (26) till $\mathcal{O}(\xi^{-1})$ and obtaining λ, the subsequent wave speed is written as

$$c_r^{(1)} = \mathrm{Re}(c^{(1)}) \sim \kappa_b^{-1}\left[1 + \frac{4}{17325}\left(\frac{k\mathrm{Pe}}{\Upsilon_b\kappa_b}\right)^2\right], \tag{32}$$

$$c_i^{(1)} = \mathrm{Im}(c^{(1)}) \sim -\frac{\Upsilon k}{\mathrm{Pe}} - \frac{2k\mathrm{Pe}}{105\Upsilon_b\kappa_b^2}. \tag{33}$$

Here, the superscript Eq. (1) specifies the wave speed corresponding to the particle mode, and the subscripts r and i denote the real and imaginary parts, respectively. The expression for $c_i^{(1)}$ has two distinct contributions, the first term coming from the Brownian diffusion, which scales as $k\mathrm{Pe}^{-1}$, whereas the second term is the Taylor dispersion term that scales as $k\mathrm{Pe}$. Thus Brownian diffusion would have the leading contribution for $\mathrm{Pe} < 1$. However, with a large Pe, Taylor dispersion dominates.

Next we consider the opposite limit, $\xi \to 0$ ($k\mathrm{Pe} \to \infty$). Inspecting the analytical solution provided by Eq. (29), this limit implies $z \to -\infty$. Thus the complex wave speed is

$$c_r^{(1)} \sim 3\kappa_b^{-1}\left[\frac{1}{2} - \left(n + \frac{1}{2}\right)\sqrt{\xi}\right], \tag{34}$$

$$c_i^{(1)} \sim -\frac{\Upsilon k}{\mathrm{Pe}} - \left(n + \frac{1}{2}\right)\frac{3\sqrt{\xi}}{\kappa_b}. \tag{35}$$

The contribution of the Brownian diffusion is visible from the first term alongside another that encompasses the anomalous modes as described by Camassa *et al.* [56]. Further, as the ratio between the two goes as $\sqrt{\mathrm{Pe}/k^3}$, we can infer that the value of Pe has to be large for the anomalous modes to dominate. Thus Pe can be seen to play an essential role in dictating the occurrence of transitions between the different classes of modes while otherwise being dominated predominantly by the Brownian diffusion in the small to order one Pe range.

TABLE I. Estimates of physical parameters in a particle-laden falling film.

Parameter	Value
Film thickness, h_0 (m)	10^{-5}–10^{-3}
Flow length, l (m)	10^{-2}–10^{-1}
Fluid density, ρ (kg m^{-3})	$\sim 10^{3}$
Particle density, ρ_p (kg m^{-3})	$\sim 10^{3}$
Surface tension, σ (kg s^{-2})	$\sim 10^{-1}$
Fluid viscosity, μ_f (kg m^{-1} s^{-1})	10^{-3}–10^{-1}
Particle diameter, a (m)	10^{-8}–10^{-7}
Nondimensional numbers	**Value**
Film aspect ratio, $\epsilon = \frac{h_0}{l}$	$\sim 10^{-3}$–10^{-1}
Reynolds number, $\mathrm{Re} = \frac{\rho u_0 h_0}{\mu_f}$	10^{-3}–10^{1}
Weber number, $\mathrm{We} = \frac{\sigma}{\rho u_0^2 h_0}$	10^{2}–10^{8}
Capillary number, $\mathrm{Ca} = \frac{1}{\mathrm{WeRe}}$	10^{-6}–10^{-2}
Peclet number, $\mathrm{Pe} = \frac{u_0 h_0}{D_0}$	10–10^{9}
Peclet number, $\mathrm{Pe}_p = \frac{\dot{\gamma} a^2}{D_0}$	10^{-4}–10
Schmidt number, $\mathrm{Sc} = \frac{\mu_f}{\rho D_0}$	10^{5}–10^{9}

B. Surface mode

Equations (20)–(25) permit a solution devoid of particle concentration perturbation ($\hat{\phi} = 0$). Taking cues from the surface instability calculations of Yih [11], we explore the surface mode in the limit of long wavelengths ($k \ll 1$). In this limit, one can simplify the problem by expanding the variables of the problem in powers of wave number as $\hat{\psi} = \hat{\psi}_0 + k\hat{\psi}_1 \ldots$ and $c = c_0 + kc_1 \ldots$ while taking the solution $\hat{\phi} = 0$. With this, the resulting equations can be solved till $\mathcal{O}(k)$ to obtain the complex wave speed of the surface mode as

$$c^{(2)} = c_0^{(2)} + kc_1^{(2)} \cdots \sim 3\kappa_b^{-1} + ik\kappa_b^{-1}\left(\tfrac{6}{5}\kappa_b^{-2}\mathrm{Re} - \cot\alpha - \tfrac{1}{3}k^2\mathrm{We\,Re}\right). \tag{36}$$

Here, the superscript Eq. (2) is a label for the surface mode. Also, we retain the k^2We term at $\mathcal{O}(1)$ to incorporate the role of surface tension. This can be justified physically since the typical values of Weber numbers for waterlike systems are large (see Table I). We can easily verify that the second mode obtained from this linear stability calculation is similar to the one obtained by Yih [11], except for the presence of viscosity terms (κ_b) that appear as a consequence of the presence of particles. Equating $\mathrm{Im}(c) = 0$ and ignoring the surface tension term, we obtain the stability criterion to be

$$\mathrm{Re}_c = \tfrac{5}{6}\kappa_b^2 \cot\alpha, \tag{37}$$

where Re_c denotes the critical Reynolds number. The derived expressions differ from the critical Reynolds number obtained by Yih [11] with the appearance of a nondimensional viscosity term. The addition of particles increases the critical Reynolds number, thus bringing an expected stabilizing effect. This is also evident from the first term in the imaginary part of Eq. (36) as the presence of viscosity indicates a delay in the onset of instability. We therefore find that the the uniform increase in bulk viscosity of the base state along the gradient direction acts to stabilize the system. The hydrostatic pressure term and the surface tension term [second and third imaginary terms of Eq. (36)] act to stabilize the system. The plots for the different inclinations in Fig. 2(a) show how smaller inclinations tend to be more stable. It could also be seen that the increase in critical Reynolds number with an increase in particle volume fraction gets steeper in the case of smaller inclinations.

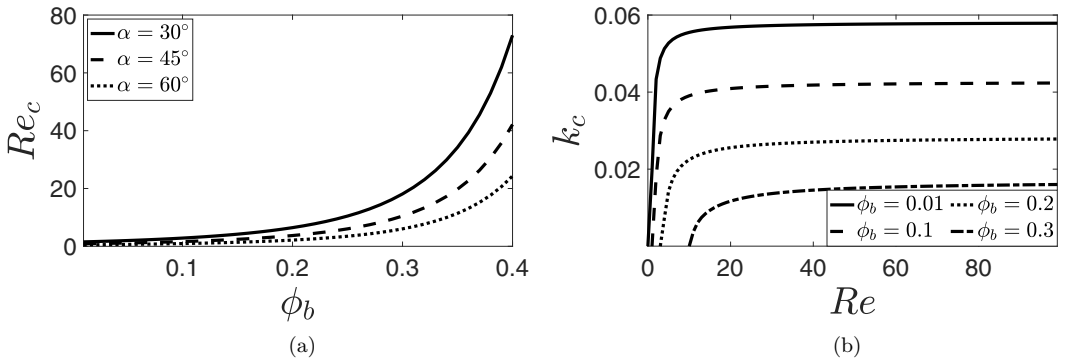

FIG. 2. (a) Critical Reynolds number for inclinations of 30°, 45°, and 60° and (b) critical wave number plotted for $\phi_b = 0.1$, 0.2, and 0.3 with inclination angle $\alpha = 45°$, We $= 10^3$.

Further, a critical wave number can also be obtained by equating the imaginary part of Eq. (36) to zero as

$$k_c = \frac{1}{\sqrt{\frac{\mathrm{We\,Re}}{3}}}\sqrt{\frac{6}{5}\kappa_b^{-2}\mathrm{Re} - \cot\alpha}. \tag{38}$$

The critical wave numbers for different values of particle volume fractions are plotted in Fig. 2(b) for inclination $\alpha = 45°$ and Weber number We $= 10^3$. The plots show that for a value of Reynolds number above Re_c and wave number $0 < k < k_c$, the system is linearly unstable. The other notable effect is with increasing particle volume fraction, the curve shift toward the right. This behavior is analogous to that of the power-law exponents in the case of a power-law fluid [59] and permeability in the case of a porous inclined plane [60].

C. Finite wave-number analysis

Next, we investigate the linear response of a colloidal falling film to infinitesimal disturbances of arbitrary wavelengths. Thus, Eqs. (20) and (21) are posed as an eigenvalue problem for c and solved numerically using a spectral collocation method [61]. Details on the numerical method used are in Appendix A. We begin by comparing the asymptotic predictions for the particle mode. Figure 3 shows the real part of numerically obtained wave speeds, c_r, compared with the asymptotic predictions (dashed lines in the insets) for both $k \ll 1$ and $k \gg 1$, keeping Pe $= 1$ fixed. There is no perceptible change in the values of c_r for a higher value of Peclet number Pe $= 1000$ (see Fig. 3—blue lines indicating the case of Pe $= 1000$ overlap the black lines indicating the case of Pe $= 1$). However, inspecting c_i in Fig. 4(a) shows how Brownian diffusion tends to dominate throughout the range of k explored for this choice of Peclet number, consistent with the discussion from the previous section. The inset of Fig. 4(a) shows further detailed comparisons. Once we subtract the dominant Brownian contribution, the subtle presence of Taylor and anomalous modes are visible. However, an increase in the Peclet number to 1000 shows a distinct transition between the three modes. For $k \ll 1$, the Taylor mode has the most dominant signature, which is then succeeded by an intermediate anomalous mode for $k \sim \mathcal{O}(1)$ and, finally, for $k \gg 1$ Brownian diffusion persists [see Fig. 4(b)]. Thus, even though the particle dynamics is purely damped, it offers rich physics. The spatial scales associated with the disturbance and the value of Pe dictate the particulate phase's dispersion. Figures 5(a)–5(f) show the eigenfunctions pertaining to the three regimes of the particle mode.

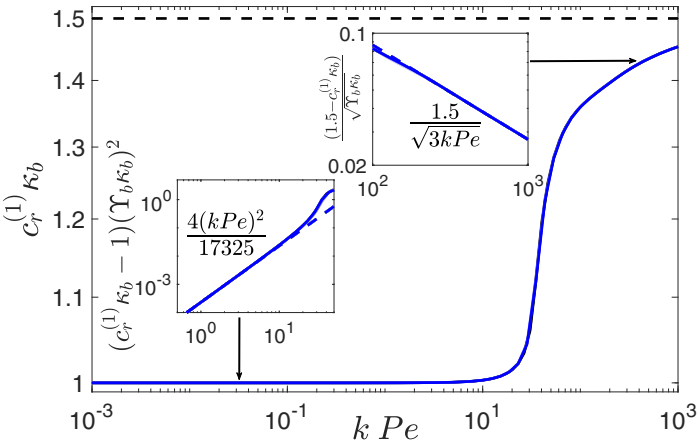

FIG. 3. Real part of wave speed corresponding to the particle mode calculated numerically for $\phi_b = 0.01$, Pe $= 1$ (black line) and Pe $= 1000$ (blue line). Comparisons with the asymptotic calculations indicated by dashed lines are shown in the inset.

We then consider the momentum Eq. (20) to probe the surface mode. As predicted by the long-wave calculations, the surface mode instability appears for small wave numbers (see Sec. III B). Exploring larger wave numbers shows the onset of another instability—the viscous Tollmien-Schlicting shear mode instability, similar to those found in plane Poisueille and Blasius boundary layer flows at large Reynolds numbers [62]. The neutral stability curves of both the interfacial and the shear modes are visible in Fig. 6. As per expectations, on increasing the particle concentration, the onset of instability is delayed. Investigating the vorticity eigenfunctions for the surface mode in Fig. 7(a) and that of the shear mode in Fig. 7(b) shows how the structure of the two modes varies from each other. The $\mathcal{O}((\mathrm{kRe})^{1/3})$ scaling of the wall-normal coordinate for the shear mode conforms with critical layer arguments [63]. Chin *et al.* [14] also noted earlier that the shear mode has a very distinct localized peak near the bottom wall. For the particle-free problem, Floryan *et al.* [15] analyzed the dynamics of the two modes in a falling film and observed that the shear mode could prevail over the surface mode only when the inclination angle is minimal.

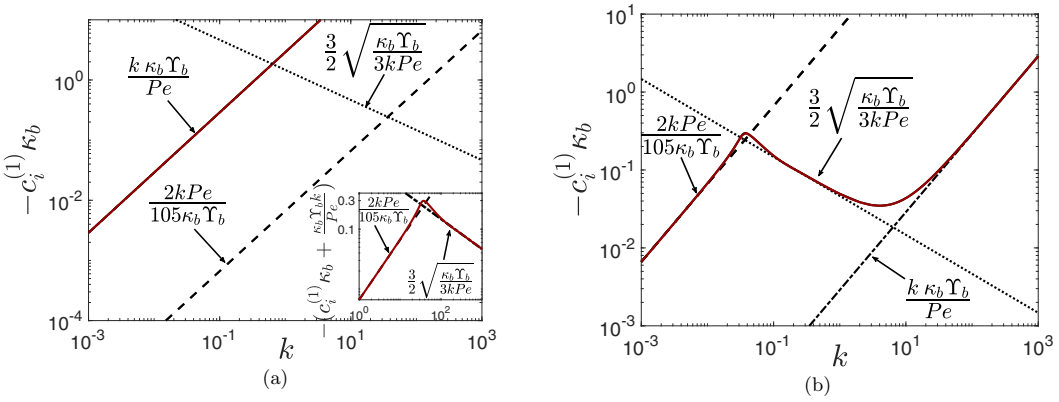

FIG. 4. Comparisons of the imaginary part of wave speed corresponding to the particle mode calculated numerically with the asymptotic calculations in black lines with (a) Pe $= 1$ and (b) Pe $= 1000$ for $\phi_b = 0.01$ and red lines indicating the corresponding numerical calculations.

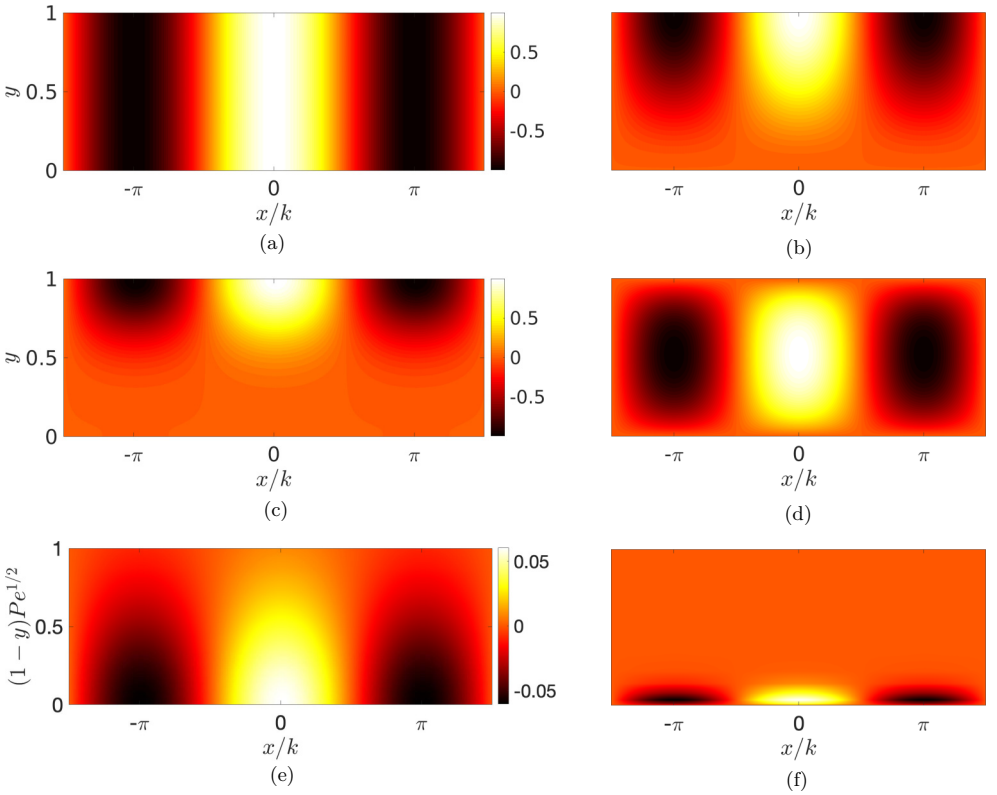

FIG. 5. Eigenfunctions of the particle mode at $t = 0.001$ for $\phi_b = 0.01$ with Pe $= 1000$. (a) Taylor mode - $\hat{\phi}; k = 0.001$, (b) Taylor mode - $\hat{\psi}; k = 0.001$, (c) Anomalous mode - $\hat{\phi}; k = 1$, (d) Anomalous mode - $\hat{\psi}; k = 1$, (e) Brownian diffusion mode - $\hat{\phi}; k = 1000$, and (f) Brownian diffusion mode - $\hat{\psi}; k = 1000$.

Thus the linear stability analysis for a colloidal falling film has revealed two features: the stabilization of the surface mode and the intricate decay dynamics of the particle mode. Next, we will try to understand the wavy dynamics of the particle-laden film in the nonlinear regime, with insights obtained from the linear stability analysis of the particle mode acting as a helpful guide.

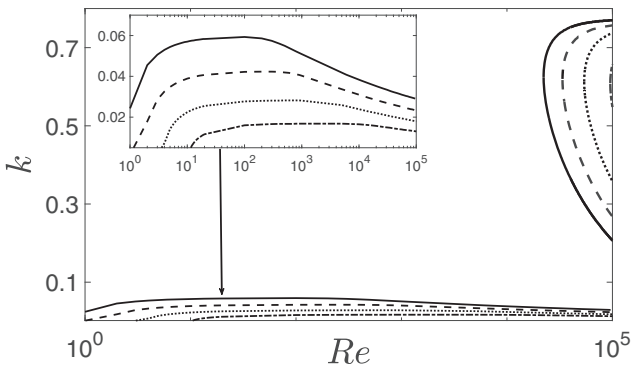

FIG. 6. Neutral stability curves corresponding to both the shear mode and the surface mode for $\phi_b = 0.01$ (—), $\phi_b = 0.1$ (- - -), $\phi_b = 0.2$ ($\cdots$), and $\phi_b = 0.3$ (-·-·-) with Pe $= 1$, $\alpha = 45^\circ$, We $= 10^3$.

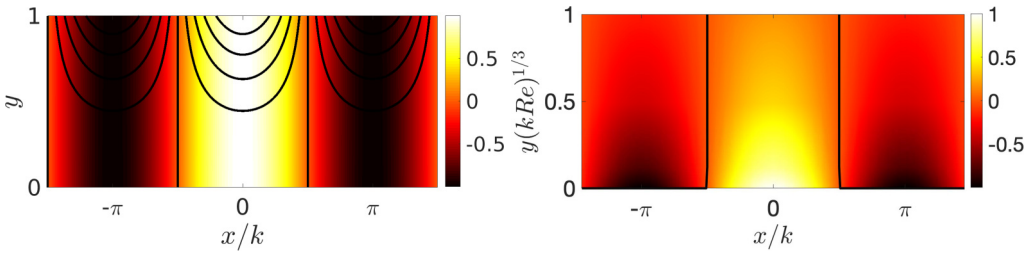

(a) $k = 0.025$, $Re = 20$ (b) $k = 0.5$, $Re = 10^6$

FIG. 7. Vorticity fields with streamlines overlaid for the surface mode (a) and shear mode (b) at $t = 0.001$ for $\phi_b = 0.01$ with Pe $= 1$, $\alpha = 45^\circ$, We $= 10^3$.

IV. NONLINEAR LONG-WAVE THEORY

A falling film of height h_0 and flow length l has a natural small parameter, $\epsilon = h_0/l$ - the film aspect ratio. Thus we carry out a long-wave scaling of the governing equations to obtain [7]

$$\frac{\partial u}{\partial x} + \frac{\partial v}{\partial y} = 0, \tag{39}$$

$$\epsilon \mathrm{Re}\left(\frac{\partial u}{\partial t} + u\frac{\partial u}{\partial x} + v\frac{\partial u}{\partial y}\right) = -\epsilon \mathrm{Re}\frac{\partial P}{\partial x} + \epsilon^2 \frac{\partial}{\partial x}\left(\kappa(\phi)\frac{\partial u}{\partial x}\right) + \frac{\partial}{\partial y}\left(\kappa(\phi)\frac{\partial u}{\partial y}\right) + \epsilon^2 \frac{\partial \kappa(\phi)}{\partial y}\frac{\partial v}{\partial x} - \epsilon^2 \frac{\partial \kappa(\phi)}{\partial x}\frac{\partial v}{\partial y} + 3, \tag{40}$$

$$\epsilon^2 \mathrm{Re}\left(\frac{\partial v}{\partial t} + u\frac{\partial v}{\partial x} + v\frac{\partial v}{\partial y}\right) = -\mathrm{Re}\frac{\partial P}{\partial y} + \epsilon^3 \frac{\partial}{\partial x}\left(\kappa(\phi)\frac{\partial v}{\partial x}\right) + \epsilon \frac{\partial}{\partial y}\left(\kappa(\phi)\frac{\partial v}{\partial y}\right) + \epsilon \frac{\partial \kappa(\phi)}{\partial x}\frac{\partial u}{\partial y} - \epsilon \frac{\partial \kappa(\phi)}{\partial y}\frac{\partial u}{\partial x} - 3\cot\alpha, \tag{41}$$

$$\epsilon \mathrm{Pe}\left(\frac{\partial \phi}{\partial t} + u\frac{\partial \phi}{\partial x} + v\frac{\partial \phi}{\partial y}\right) = \epsilon^2 \frac{\partial}{\partial x}\left(\Upsilon(\phi)\frac{\partial \phi}{\partial x}\right) + \frac{\partial}{\partial y}\left(\Upsilon(\phi)\frac{\partial \phi}{\partial y}\right). \tag{42}$$

The above equations are complemented by the boundary conditions at $y = 0$,

$$u = v = 0, \quad \frac{\partial \phi}{\partial y} = 0, \tag{43}$$

and at $y = h$

$$\mathrm{Re}\, P = \frac{2\epsilon\kappa(\phi)}{\left[1 + \epsilon^2\left(\frac{\partial h}{\partial x}\right)^2\right]}\left[\epsilon^2\left(\frac{\partial u}{\partial x}\left(\frac{\partial h}{\partial x}\right)^2 - \frac{\partial v}{\partial x}\frac{\partial h}{\partial x}\right) - \frac{\partial u}{\partial y}\frac{\partial h}{\partial x} + \frac{\partial v}{\partial y}\right] - \frac{\epsilon^2 \mathrm{We}\,\mathrm{Re}\frac{\partial^2 h}{\partial x^2}}{\left[1 + \epsilon^2\left(\frac{\partial h}{\partial x}\right)^2\right]^{3/2}},$$
$$0 = 4\kappa(\phi)\epsilon^2 \frac{\partial u}{\partial x}\frac{\partial h}{\partial x} - \kappa(\phi)\left(1 - \epsilon^2\left(\frac{\partial h}{\partial x}\right)^2\right)\left(\frac{\partial u}{\partial y} + \epsilon^2 \frac{\partial v}{\partial x}\right), \quad \epsilon^2 \Upsilon(\phi)\frac{\partial h}{\partial x}\frac{\partial \phi}{\partial x} - \Upsilon(\phi)\frac{\partial \phi}{\partial y} = 0. \tag{44}$$

Now we adopt an approach that is often used for problems in falling film dynamics [7], performing a perturbative expansion of the physical variables u, v, p, and ϕ,

$$u = u_0 + \epsilon u_1 ..., \quad v = v_0 + \epsilon v_1 ...,$$
$$P = P_0 + \epsilon P_1 ..., \quad \phi = \phi_0 + \epsilon \phi_1 ... \tag{45}$$

On substituting the above expansions, the leading order expression for the particle concentration, with the no-flux boundary conditions, reveals the dominance of the vertical diffusion. Thus diffusion equilibrates the particle concentration in the gradient direction, provided $\epsilon \mathrm{Pe} \ll 1$, implying ϕ is independent of y at this order. This allows us to write the leading order velocity as

$$u_0 = \frac{3}{\kappa(\phi_0)}\left(yh - \frac{y^2}{2}\right). \tag{46}$$

Following the work of Espin and Kumar [37], it is possible to write an equation for the particle concentration field under the assumption that Pe is an $\mathcal{O}(\epsilon)$ quantity. This assumption is crucial in to retain the diffusion term. It must be noted that the definition of Peclet number as written by Espin and Kumar [37] is equivalent to Pe/ϵ as defined here. With the particle concentration field being invariant along the gradient direction, it can be decomposed as $\phi(x, y, t) = \phi_{00}(x, t) + \mathcal{O}(\epsilon \mathrm{Pe})$. Upon substitution of this decomposition in Eq. (42) and integrating across the film height to drop all y dependencies, we obtain

$$\frac{\partial(h\phi_{00})}{\partial t} + \frac{\partial(q\phi_{00})}{\partial x} = \frac{\epsilon}{\mathrm{Pe}}\frac{\partial}{\partial x}\left(\Upsilon(\phi_{00})h\frac{\partial \phi_{00}}{\partial x}\right). \tag{47}$$

Here $q = \int_0^h u dy$ denotes the flow rate. As stated earlier, the above equation requires Pe to be a small quantity. However, in the present study of a colloidal falling film, the Peclet number, based on film thickness as a characteristic length scale, can be large (see Table I). Also, we previously observed (Sec. III A) that in the limit of small wave numbers and large Peclet numbers, Taylor dispersion dominates over molecular diffusion. Thus we proceed to incorporate the Taylor dispersion component in the nonlinear wave equation for a falling film by using the central manifold approach. Roberts [64] and Mercer and Roberts [53] previously used a similar approach to study contaminant transport in conduits with spatially varying cross-sectional areas. For this, we first write the volume fraction evolution equation as

$$\mathcal{L}\phi = \epsilon \mathrm{Pe}\left(\frac{\partial \phi}{\partial t} + u\frac{\partial \phi}{\partial x} + v\frac{\partial \phi}{\partial y}\right) - \epsilon^2 \frac{\partial}{\partial x}\left(\Upsilon \frac{\partial \phi}{\partial x}\right), \tag{48}$$

where $\mathcal{L} = \Upsilon \partial^2/\partial y^2$ is the linear operator. For simplicity, the Brownian diffusivity term (Υ) is taken as a function of the depth-averaged concentration field $\bar{\phi}(x, t)$. This is complemented by the no-flux boundary conditions at both the bottom substrate and the free interface. With this system, assuming that the variations along x and t happen over large length and time scales, the volume fraction can be described by a cross-section averaged volume fraction noted as $\bar{\phi}(x, t)$. We thus proceed to describe the center manifold as

$$\phi = V[y; \bar{\phi}], \tag{49}$$

with the evolution on the center manifold given by

$$\frac{\partial \bar{\phi}}{\partial t} = G[\bar{\phi}]. \tag{50}$$

Here, the square brackets denote that the quantities have a functional dependence on $\bar{\phi}$ and its derivatives with respect to x. Assuming slow variations along x and t, we write an asymptotic

expansion of the form

$$V \approx \sum_{n=0}^{\infty} \epsilon^n V^n \qquad G \approx \sum_{n=0}^{\infty} \epsilon^n G^n, \tag{51}$$

where $n = 1, 2, \ldots$. To proceed with the analysis, we also require knowledge of the velocity field. As noted by Mercer and Roberts [53], it is convenient to fix a velocity profile to evaluate ϕ at higher orders. Therefore, inspired by the leading order velocity field Eq. (46), we consider the fluid flow to be a quasi-Nusselt flow velocity as

$$u \sim \frac{3q}{h}\left(\bar{y} - \frac{\bar{y}^2}{2}\right). \tag{52}$$

The particle concentration evolution is subsequently written in different orders as

$$\begin{aligned}
&\mathcal{L}V^0 = 0,\\
&\mathcal{L}V^n = \epsilon \mathrm{Pe}\left(V_t^{n-1} + \sum_{l=1}^{n}\sum_{p=0}^{n-l} V_{\phi^{(p)}} \frac{\partial^p G^l}{\partial x^p} + u\frac{\partial V^{n-1}}{\partial x} + v\frac{\partial V^{n-1}}{\partial y}\right) - \epsilon^2 \frac{\partial}{\partial x}\left(\Upsilon \frac{\partial V^{n-2}}{\partial x}\right).
\end{aligned} \tag{53}$$

With the calculations done till $n = 2$, the particle volume fraction obtained is

$$\begin{aligned}
\phi &\approx V^0 + \epsilon V^1 + \epsilon^2 V^2\\
&= \bar{\phi} + \epsilon h q \frac{\mathrm{Pe}}{\Upsilon}\left(\frac{1}{15} - \frac{\bar{y}^2}{2} + \frac{\bar{y}^3}{2} - \frac{\bar{y}^4}{8}\right)\frac{\partial \bar{\phi}}{\partial x} + \epsilon^2 h\left(\frac{\bar{y}^2}{2} - \frac{1}{6}\right)\frac{\partial h}{\partial x}\frac{\partial \bar{\phi}}{\partial x}\\
&\quad + \epsilon^2 h^2 q \frac{\mathrm{Pe}^2}{\Upsilon^2}\left(-\frac{1}{315} + \frac{\bar{y}^2}{240} + \frac{\bar{y}^4}{24} - \frac{\bar{y}^5}{20} + \frac{\bar{y}^6}{80}\right)\frac{\partial h}{\partial t}\frac{\partial \bar{\phi}}{\partial x}\\
&\quad + \epsilon^2 h^3 \frac{\mathrm{Pe}^2}{\Upsilon^2}\left(-\frac{2}{315} + \frac{\bar{y}^2}{30} - \frac{\bar{y}^4}{24} + \frac{\bar{y}^5}{40} - \frac{\bar{y}^6}{240}\right)\frac{\partial q}{\partial t}\frac{\partial \bar{\phi}}{\partial x}\\
&\quad + \epsilon^2 h q^2 \frac{\mathrm{Pe}^2}{\Upsilon^2}\left(-\frac{4}{225} + \frac{8\bar{y}^2}{105} + \frac{\bar{y}^3}{30} - \frac{11\bar{y}^4}{120} - \frac{\bar{y}^5}{40} + \frac{\bar{y}^6}{15} - \frac{3\bar{y}^7}{112} + \frac{3\bar{y}^8}{896}\right)\frac{\partial h}{\partial x}\frac{\partial \bar{\phi}}{\partial x}\\
&\quad + \epsilon^2 h^2 q \frac{\mathrm{Pe}^2}{\Upsilon^2}\left(\frac{17}{1575} - \frac{43\bar{y}^2}{560} + \frac{\bar{y}^3}{30} + \frac{3\bar{y}^4}{40} - \frac{\bar{y}^5}{20} - \frac{\bar{y}^6}{120} + \frac{\bar{y}^7}{112} - \frac{\bar{y}^8}{896}\right)\frac{\partial q}{\partial x}\frac{\partial \bar{\phi}}{\partial x}\\
&\quad + \epsilon^2 h^2 (1 - \mathrm{Pe})\left(\frac{1}{6} - \frac{\bar{y}^2}{2}\right)\frac{\partial^2 \bar{\phi}}{\partial x^2} + \epsilon^2 q^2 h^2 \frac{\mathrm{Pe}^2}{\Upsilon^2}\left(\frac{4}{525} - \frac{2\bar{y}^2}{35} + \frac{\bar{y}^3}{30} + \frac{3\bar{y}^4}{40}\right.\\
&\quad \left. - \frac{\bar{y}^5}{8} + \frac{\bar{y}^6}{12} - \frac{3\bar{y}^7}{112} + \frac{3\bar{y}^8}{896}\right)\frac{\partial^2 \bar{\phi}}{\partial x^2} + \epsilon^2 h^2 \frac{\Upsilon_{\bar{\phi}}}{\Upsilon}(1 - \mathrm{Pe})\left(\frac{1}{6} - \frac{\bar{y}^2}{2}\right)\left(\frac{\partial \bar{\phi}}{\partial x}\right)^2\\
&\quad + \epsilon^2 q^2 h^2 \frac{\mathrm{Pe}^2 \Upsilon_{\bar{\phi}}}{\Upsilon^3}\left(-\frac{2}{1575} + \frac{\bar{y}^2}{42} - \frac{\bar{y}^3}{30} - \frac{\bar{y}^4}{30} + \frac{\bar{y}^5}{10} - \frac{19\bar{y}^6}{240} + \frac{3\bar{y}^7}{112} - \frac{3\bar{y}^8}{896}\right)\left(\frac{\partial \bar{\phi}}{\partial x}\right)^2.
\end{aligned} \tag{54}$$

Here, $\Upsilon_{\bar{\phi}} = d\Upsilon(\bar{\phi})/d\bar{\phi}$. Subsequently, the evolution of the depth-averaged particle volume fraction field becomes

$$\begin{aligned}
\frac{\partial \bar{\phi}}{\partial t} &\approx G^1 + \epsilon G^2\\
&= -\frac{q}{h}\frac{\partial \bar{\phi}}{\partial x} + \epsilon \frac{1}{\mathrm{Pe}}\frac{\partial}{\partial x}\left(\Upsilon \frac{\partial \bar{\phi}}{\partial x}\right) + \epsilon \frac{\Upsilon}{\mathrm{Pe}}\frac{\partial h}{\partial x}\frac{\partial \bar{\phi}}{\partial x}\\
&\quad + \epsilon \frac{\mathrm{Pe}}{\Upsilon}\left(\frac{2}{105}q^2\frac{\partial^2 \bar{\phi}}{\partial x^2} + \frac{2}{105}\frac{q^2}{h}\frac{\partial \bar{\phi}}{\partial x}\frac{\partial h}{\partial x} - \frac{2}{105}q^2\frac{\Upsilon_{\bar{\phi}}}{\Upsilon}\left(\frac{\partial \bar{\phi}}{\partial x}\right)^2 + \frac{4}{105}q\frac{\partial \bar{\phi}}{\partial x}\frac{\partial q}{\partial x}\right).
\end{aligned} \tag{55}$$

Appendix B has the detailed derivation of V^n, and G^n evaluated till $n = 2$. The above can be rewritten in the conservative form as

$$\frac{\partial(h\bar{\phi})}{\partial t} + \frac{\partial(q\bar{\phi})}{\partial x} = \epsilon \frac{\partial}{\partial x}\left\{\left(\frac{\Upsilon(\bar{\phi})}{\mathrm{Pe}}h + \frac{2\mathrm{Pe}}{105}\frac{q^2 h}{\Upsilon(\bar{\phi})}\right)\frac{\partial \bar{\phi}}{\partial x}\right\}. \tag{56}$$

It should be noted that the above equation is similar to the one obtained by Mercer and Roberts [53] for studying contaminant transport in a channel with spatially varying width. The $n > 2$ terms are responsible for incorporating higher-order models of Taylor dispersion [53,65]. Suppose one were to do this calculation for a constant film thickness (flat film with a half-parabolic flow profile), the evolution equation for the depth-averaged particle volume fraction will remain the same as Eq. (56), but with h and q being constants.

With the particle volume fraction field now evaluated, we proceed to calculate the $\mathcal{O}(\epsilon)$ correction to the flow rate. For this, we use the evaluated particle concentration field till $\mathcal{O}(\epsilon)$ [first two lines of Eq. (54)] and derive an expression for the flow rate

$$q = \kappa^{-1}h^3\Bigg[1 - \epsilon\left(\cot\alpha\frac{\partial h}{\partial x} - \frac{\epsilon^2\mathrm{WeRe}}{3}\frac{\partial^3 h}{\partial x^3}\right) + \epsilon\mathrm{Re}\kappa^{-2}\left(\kappa_{\bar{\phi}}\frac{2}{5}h^2\frac{\partial\bar{\phi}}{\partial t} - \kappa^{-1}\kappa_{\bar{\phi}}\frac{8}{35}h^4\frac{\partial\bar{\phi}}{\partial x} + \frac{6}{5}h^3\frac{\partial h}{\partial x}\right)$$
$$- \epsilon\kappa^{-2}\kappa_{\bar{\phi}}\frac{4}{105}h^4\frac{\mathrm{Pe}}{\Upsilon(\bar{\phi})}\frac{\partial\bar{\phi}}{\partial x}\Bigg], \tag{57}$$

with the evolution of the film height described by

$$\frac{\partial h}{\partial t} + \frac{\partial q}{\partial x} = 0. \tag{58}$$

Here, $\kappa_{\bar{\phi}} = d\kappa(\bar{\phi})/d\bar{\phi}$. As previously mentioned in Sec. III B, we retain the ϵ^2We term at $\mathcal{O}(1)$ to incorporate the role of surface tension. The above Eqs. (58) and (57) coupled with Eq. (56) form the modified Benney system of equations. To study the linear stability of the above model equations, the equations are linearized as previously done in Sec. III. The resulting set of linear equations can be subsequently solved for c to obtain

$$c^{(1)} = \kappa_b^{-1} - i\epsilon k\left(\frac{\Upsilon_b}{\mathrm{Pe}} + \frac{2}{105}\frac{\kappa_b^{-2}\mathrm{Pe}}{\Upsilon_b}\right), \tag{59}$$

$$c^{(2)} = 3\kappa_b^{-1} + i\epsilon k\kappa_b^{-1}\left(\frac{6}{5}\kappa_b^{-2}\mathrm{Re} - \cot\alpha - \frac{\mathrm{We\,Re}}{3}\epsilon^2 k^2\right). \tag{60}$$

It is immediately evident that for $\epsilon \to 1$, we recover the wave speed expressions that were obtained from the previous linear stability calculation in Sec. III for the surface mode ($c^{(2)}$). Also, the expression for the wave speed corresponding to the particle mode ($c^{(1)}$) bears resemblance to Eqs. (32) and (33). The linear stability analysis of the complete system (Sec. III), when analyzed in the limit of $\mathrm{Pe} \ll 1$, highlighted the dominance of Brownian diffusion. Instead, suppose we were interested in larger values of Peclet numbers. In that case, the role of Taylor dispersion becomes crucial. However, the restriction for the model to be valid dictates that Pe has to be a $\mathcal{O}(1)$ quantity. In the Stokesian limit ($\mathrm{Re} = 0$), a modal linear stability analysis indicates that the particle-laden film is exponentially stable [$\mathrm{Im}(c) < 0$]. However, the solution of the linear initial value problem (IVP) reveals the possibility of a transient algebraic growth of disturbances. linearizing the Eqs. (56)– (58) with $h = 1 + \delta h_1(t)e^{ikx}$ and $\bar{\phi} = \phi_b(1 + \delta\bar{\phi}_1(t)e^{ikx})$, where $\delta \ll 1$, in the limit of $\mathrm{Re} = 0$, we obtain the following solution:

$$h = 1 + \delta\,\Re\left[h_1(0)e^{ik(x-c^{(2)}t)} + \kappa_{b1}\phi_b\frac{e^{-ikc^{(2)}t} - e^{-ikc^{(1)}t}}{c^{(2)} - c^{(1)}}e^{ikx}\right] \tag{61}$$

$$\bar{\phi} = \phi_b + \delta\,\Re[\phi_b\bar{\phi}_1(0)e^{ik(x-c^{(1)}t)}], \tag{62}$$

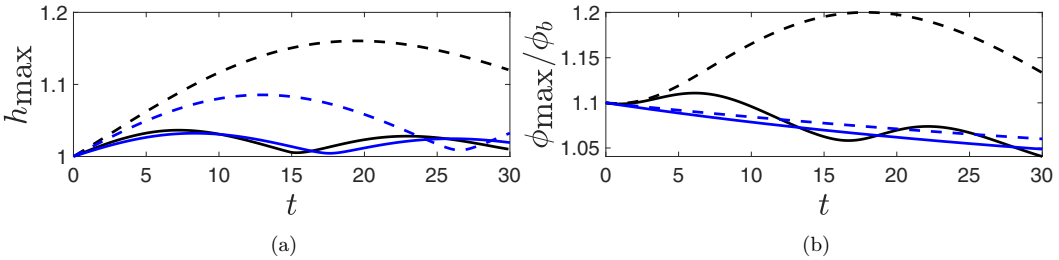

FIG. 8. Evolution of film height h and particle concentration ϕ for the zero-inertia system with $k = 0.25$ and $\mathrm{Pe} = 1$ for $\phi_b = 0.1$ (—) and $\phi_b = 0.2$ (- - -); $\alpha = 45^\circ$, $\mathrm{We} = 10^3$. The blue lines indicate the solution of the linear IVP for the corresponding cases.

where $c^{(1)}$ and $c^{(2)}$ are the complex wave speeds of the particle and surface mode respectively [see Eqs. (59) and (60)]. The linear IVP solution is then compared with the solution of the full nonlinear system [Eqs. (56)–(58)]. To retain the surface tension terms, we replace We Re with Ca^{-1}. The nonlinear equations are solved numerically with the initial concentration field taken as $\bar{\phi}(x, 0) = \phi_b(1 - 0.1\cos kx)$, leaving the initial height unperturbed. We perform the numerical calculations with $\epsilon = 0.2$, $\mathrm{Ca} = 10^{-3}$ and $\mathrm{Pe} = 1$ since switching to a viscous scaling for pressure would indeed give us Ca. Figure 8 shows the evolution of the maximum film height ($h_{\max}$, the maximum value of $h(x, t)$ for $x \in [-\pi/k, \pi/k]$) and maximum particle volume fraction ($\phi_{\max}$, the maximum value of $\bar{\phi}(x, t)$ for $x \in [-\pi/k, \pi/k]$) for $\phi_b = 0.1$ and 0.2 while excited with perturbations of wave number $k = 0.25$. The height perturbations grow as predicted by the nonmodal linear stability analysis. However, the concentration field decays as expected before further growth, with the nonlinear effects becoming prominent.

A. Role of fluid inertia

The inclusion of fluid inertia can destabilize the surface mode, subject to the criticality conditions as shown in Sec. III. With the linear stability calculations predicting the critical wav number (k) and Reynolds number (Re) for a given set of parameters, we next carry out nonlinear calculations by exciting the surface mode beyond this threshold of instability. We previously learned in Sec. III that the perturbation equations in the linear limit are a one-way coupled system, i.e., the velocity perturbations can affect the particle volume fraction perturbations, but not the other way around. Therefore, since we are interested in triggering the surface mode, we initialize the film with an initial height $h(x, 0) = 1-0.1\cos(kx)$, leaving the concentration field unperturbed. With this, the evolution Eqs. (56)– (58) are solved numerically with $\epsilon = 0.2$ and $\mathrm{Pe} = 1$.

For disturbances that are close to the critical wave number k_c, the waves increase in amplitude and then subsequently evolve into small amplitude waves with an almost sinusoidal signature [59,66]. The maximum growth rate occurs at $k_m = k_c/\sqrt{2}$ [9]. The black lines in Fig. 9 show the evolution of maximum film height ($h_{\max}$) and maximum particle volume fraction ($\phi_{\max}$) for $\phi_b = 0.01$ and 0.1, when triggered with disturbances of wave numbers marginally lower than k_c, $k = 0.25$ and 0.15, respectively. The disturbance initially grows according to the linear growth rate, followed by a decay in amplitude. We learned earlier that an increase in ϕ_b leads to a stabilizing effect ($\phi_b \uparrow \mathrm{Im}(c) \downarrow$); thus, the concentration field has a faster growth with decreasing ϕ_b [see Fig. 9(b)]. We are solving for a two-way coupled system; an enhancement in the particle concentration field would increase the viscosity and thus stabilize the nonlinear regime of the surface mode [see Eqs. (57) and (58)]. Thus we observe an interesting feature due to this coupled nonlinear dynamics—with increasing ϕ_b, $h_{\max}$ achieves a delayed and enhanced peak. To check this hypothesis, we compare the predictions of the two-way coupled system [Eqs. (56)–(58)] with its corresponding one-way coupled system (red lines in Fig. 9). For the one-way coupled system, we modify Eqs. (56)–(58) by allowing the fluid velocity

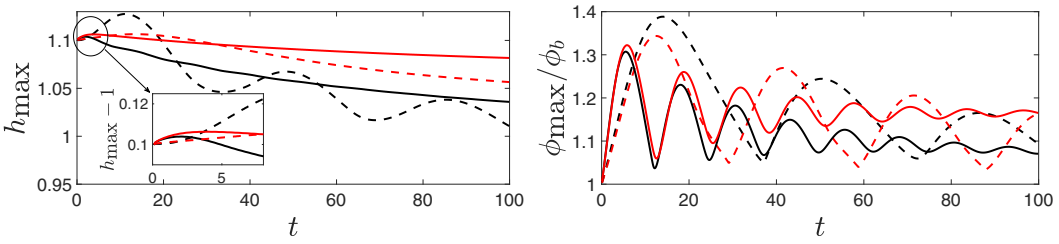

FIG. 9. Comparisons of $h_{\max}$ and $\phi_{\max}/\phi_b$ between the one-way coupled simulations (red lines) and two-way coupled simulations (black lines) with Re $= 6$, We $= 10^3$, inclination $\alpha = 45^\circ$ and $k \approx k_c$ for the corresponding initial particle concentrations (—) $\phi_b = 0.01$; (− − −) $\phi_b = 0.1$. Inset in (a) shows the initial growth of the height perturbation $h_{\max} - 1$.

to affect the particle concentration field, but not the other way around. Unlike the two-way coupled system, we no longer see the enhanced peak that we observe for the higher particle concentration with the one-way coupled system [red lines in Fig. 9(a)].

B. Boundary layer equations and depth-averaged model

Benney's long-wave equation is a useful low-dimensional model for studying the nonlinear saturation and the formation of solitary waves in an unstable falling film, provided the effects of fluid inertia are weak. Benney's approach allows for long waves of arbitrary amplitudes, and thus the flow rate is enslaved to the instantaneous local height, $q = f(h)$, resulting in a high degree of nonlinearities. This feature is responsible for finite time blowups in the solutions at moderate Reynolds number [17], which persists even for the particle-laden Benney Eqs. (57) and (58). To alleviate this singularity, we attempt alternative modeling when effects of fluid inertia are strong, adopting the approach of Ruyer-Quil and Manneville [67], popularly known as weighted residual methods [9]. We consider the nondimensional Eqs. (39)–(42), ignore the $\mathcal{O}(\epsilon^2)$ terms and then integrate the $y-$ momentum equation to obtain the expression for pressure. The expression for pressure is then substituted in the $x-$ momentum equation to obtain an expression that is consistent until $\mathcal{O}(\epsilon)$:

$$\epsilon \mathrm{Re}\left(\frac{\partial u}{\partial t} + u\frac{\partial u}{\partial x} + v\frac{\partial u}{\partial y}\right) - \frac{\partial}{\partial y}\left(\kappa(\phi)\frac{\partial u}{\partial y}\right) = -3\epsilon \cot\alpha \frac{\partial h}{\partial x} + \epsilon^3 \,\mathrm{We}\,\mathrm{Re}\frac{\partial^3 h}{\partial x^3} + 3. \tag{63}$$

This is complemented with the boundary conditions at $y = 0$,

$$u = v = 0, \quad \frac{\partial \phi}{\partial y} = 0, \tag{64}$$

and at the free surface $y = h$:

$$\frac{\partial u}{\partial y} = 0, \quad -\Upsilon(\phi)\frac{\partial \phi}{\partial y} = 0. \tag{65}$$

We subsequently decompose the velocity and concentration fields as

$$u = u_0 + \epsilon u_1, \tag{66}$$

$$\phi = \phi_0 + \epsilon \phi_1. \tag{67}$$

Here, we make the following ansatz for u_0 along the method outlined by Ruyer-Quil and Manneville [67]:

$$u_0(x, y, t) = a_0(x, t) f_0(\bar{y}), \tag{68}$$

where $f_0(\bar{y})$ is taken to be the base steady-state modified Nusselt flow solution given as

$$f_0(\bar{y}) = \frac{3}{\kappa(\phi)}\left(\bar{y} - \frac{\bar{y}^2}{2}\right). \tag{69}$$

As argued in Sec. IV, the volume fraction field ϕ in the above expression is solely a function of x and t. On using the expression, the flow rate, $q = \int_0^h u dy$, and the constraint condition $\int_0^h u_1 dy = 0$, we arrive at

$$a_0 = \frac{\kappa q}{h}. \tag{70}$$

The expression for u_0 here is similar to the quasi-Nusselt flow velocity profile considered for the derivation of the Taylor dispersion equation [see Eq. (52)]. In the derivation of the Taylor dispersion equation, we assume that the velocity profile does not deviate from a parabolic profile. However, higher-order corrections to u_0 could create deviations from the parabolic profile under the influence of fluid inertia [68]. In this analysis, we do not calculate any such higher-order corrections as we will find that u_0 is sufficient to write the equation consistent till $\mathcal{O}(\epsilon)$. Next, the weighted residuals are obtained by multiplying the equation with a suitable weight function and integrating along the depth of the film. For choosing the weight function, the Galerkin method is followed [67], which dictates that the weight function w to be used must be the test function itself, such that $w = f_0$. It also turns out that the first-order correction term u_1 gets canceled out by this choice of weight function. Using this weight function and substituting for ϕ till $\mathcal{O}(\epsilon)$ from Eq. (54), followed by subsequent integration, the evolution equation for q is obtained as

$$\begin{aligned}\epsilon \mathrm{Re}\frac{\partial q}{\partial t} = \frac{5}{2}h - \frac{5}{2}\kappa(\bar{\phi})\frac{q}{h^2} + \epsilon \mathrm{Re}\left(\frac{9}{7}\frac{q^2}{h^2}\frac{\partial h}{\partial x} - \frac{17}{7}\frac{q}{h}\frac{\partial q}{\partial x}\right) + \epsilon\frac{\mathrm{Pe}}{\Upsilon(\bar{\phi})}\frac{2}{21}\kappa_{\bar{\phi}}\frac{q^2}{h}\frac{\partial \bar{\phi}}{\partial x} \\ + \epsilon\left(-\frac{5}{2}\cot\alpha h\frac{\partial h}{\partial x} + \frac{5}{6}\epsilon^2\,\mathrm{We}\,\mathrm{Re}\,h\frac{\partial^3 h}{\partial x^3}\right).\end{aligned} \tag{71}$$

The above equation in conjunction with the equation for the film height h given by

$$\frac{\partial h}{\partial t} + \frac{\partial q}{\partial x} = 0 \tag{72}$$

can be solved to obtain the height profiles. Here, Eqs. (71) and (72) form the IBL model. Since ϕ is only a function of x and t, the evolution of the particle concentration is governed by the Taylor dispersion Eq. (56).

In the absence of particles, the nondimensional part of the viscosity $\kappa(\phi = 0) = 1$, reducing Eq. (71) to the equation obtained for a clear falling film by Ruyer-Quil and Manneville [67]. A check for consistency with the previously obtained modified Benney equation can be done by performing an expansion of the flow rate as $q = q_0 + \epsilon q_1 + ...$ in Eqs. (71) and (72) and deriving the flow rate at $\mathcal{O}(1)$ and $\mathcal{O}(\epsilon)$ as

$$q_0 = \kappa^{-1}h^3, \tag{73}$$

$$\begin{aligned}q_1 = \kappa^{-1}h^3\Bigg[-\left(\cot\alpha\frac{\partial h}{\partial x} - \frac{\epsilon^2\mathrm{WeRe}}{3}\frac{\partial^3 h}{\partial x^3}\right) + \mathrm{Re}\Bigg(-(\kappa^{-1})_t\frac{2}{5}h^2 + \kappa^{-1}(\kappa^{-1})_x\frac{8}{35}h^4 \\ + \kappa^{-2}\frac{6}{5}h^3\frac{\partial h}{\partial x}\Bigg) - \kappa^{-2}\kappa_{\bar{\phi}}\frac{4}{105}h^4\frac{\mathrm{Pe}}{\Upsilon(\bar{\phi})}\frac{\partial \bar{\phi}}{\partial x}\Bigg],\end{aligned} \tag{74}$$

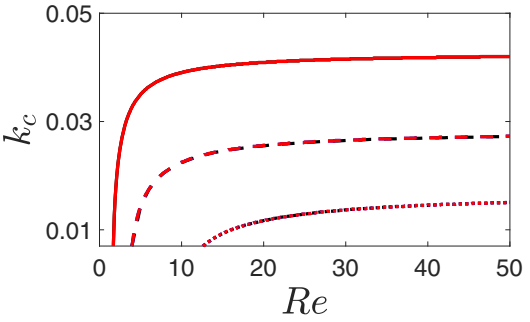

FIG. 10. Neutral stability curves corresponding to the surface mode compared between linearized Benney equations (blue lines), linearized IBL equations (red lines), and linear stability analysis (black lines) for $\phi_b = 0.1$ (—), $\phi_b = 0.2$ (- - -), and $\phi_b = 0.3$ ($\cdots$) with We $= 10^3$ and inclination $\alpha = 45^\circ$.

and subsequently writing the above in the form

$$\frac{\partial h}{\partial t} + \frac{\partial}{\partial x}(q_0 + \epsilon q_1) = 0, \tag{75}$$

the modified Benney equation [Eq. (58)] is obtained. We would like to draw the attention of the reader to a caveat of the present paper—here the entire model is restricted till $\mathcal{O}(\epsilon)$. This is unlike the second-order models as was previously derived by Ruyer-Quil and Manneville [67], Samanta *et al.* [68], where the inertia terms are evaluated till $\mathcal{O}(\epsilon^2)$. This is because a second-order model would demand evaluation of higher-order Taylor dispersion terms in the particle volume fraction evolution Eq. (56). We do not look into this aspect in the current paper.

1. Linear stability of the particle-IBL equations

Before proceeding on to the nonlinear simulations, we carry out another consistency check of the IBL equations by performing a linear stability analysis of the model equations. This is done by considering the base state as one with a flat film ($h = 1$) and constant particle concentration ($\bar{\phi} = \phi_b$) and perturbing it, just as was done in the case of the modified Benney equation [Eqs. (59) and (60)]. The linearized equations are solved for the wave speed c to obtain

$$c^{(1)} = \kappa_b^{-1} - i\epsilon k\left(\frac{\Upsilon_b}{\mathrm{Pe}} + \frac{2}{105}\frac{\kappa_b^{-2}\mathrm{Pe}}{\Upsilon_b}\right), \tag{76}$$

$$c^{(2)} = \frac{17}{14\kappa_b} + i\left\{-\frac{5\kappa_b}{4\epsilon k\mathrm{Re}} \pm \sqrt{-\frac{5\cot\alpha}{2\mathrm{Re}} - \frac{125i}{28\epsilon k\mathrm{Re}} - \frac{5}{6}\epsilon^2 k^2\mathrm{We} - \frac{37}{196\kappa_b^2} + \frac{25\kappa_b^2}{16\epsilon^2 k^2\mathrm{Re}^2}}\right\}. \tag{77}$$

As expected, the wave speed corresponding to the concentration equation [Eq. (76)] remains the same as the one obtained previously as the particle mode [Eq. (59)] and is a decaying mode. The mode dictated by the wave speed given by Eq. (77) is, however, a growing mode.

The accuracy check of the two reduced-order models is done by comparing the numerically obtained neutral stability curves (from Sec. III) with the ones obtained from the linear Benney and IBL calculations. Figure 10 shows a favorable comparison between the linear Benney calculations, linear IBL calculations, and the numerical predictions of the Orr-Sommerfeld analysis for different concentrations since the neutral stability conditions tend to occur at small wave numbers. Figure 11 displays the comparisons for the real part of the wave speed $c^{(2)}$ for concentrations $\phi_b = 0.1, 0.2$, and 0.3. We observe good agreement between the two reduced-order models and the Orr-Sommerfeld analysis in the long-wave limit. Similar observations can be made for comparisons of the corresponding imaginary part in Fig. 12. However, as one moves from the small wave-number limit, the

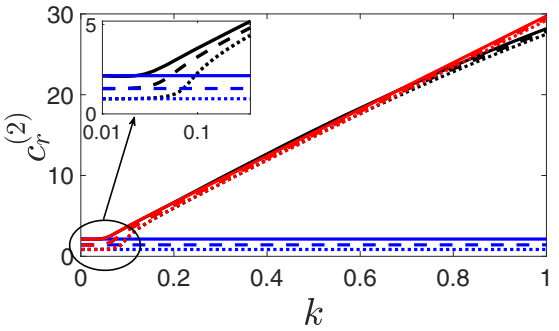

FIG. 11. Comparison of wave speed between linearized Benney equations (blue lines), linearized IBL equations (red lines), and linear stability analysis (black lines) for the case of Re = 20, (—) $\phi_b = 0.1$, (- - -) $\phi_b = 0.2$, and (· · ·) $\phi_b = 0.3$ with We = 10^3 and $\alpha = 45°$.

IBL model can be seen to have a marked improvement in terms of the range of validity over the modified Benney equations.

2. Nonlinear analysis of the particle-IBL equations

In this section, we study the full nonlinear solutions of the IBL equations, subjected to an initial finite-amplitude sinusoidal wave: $h(x, 0) = 1 - 0.1\cos(kx)$. The set of evolution Eqs. (56), (71), and (72) are subsequently solved numerically. We choose the parameters other than the Reynolds number to be the same as in the previous analysis (see Sec. IV A). In the case of Reynolds number, the modified Benney equation is valid only for $\mathcal{O}(1)$ values; however, the IBL equations stretch this validity threshold further. Here we choose Re = 12. As done previously with the modified Benney system, the simulations are studied for volume fractions $\phi_b = 0.01$ and 0.1 with the wave numbers of the disturbance chosen as before to be marginally lower than k_c as $k = 0.27$ and 0.19, respectively. Figure 13 shows the maximum film height $h_{\max}$ and maximum particle volume fraction $\phi_{\max}$ plotted over time for Pectlet numbers Pe = 1 and 2. We find that the disturbances grow initially in accordance with the linear growth rate and subsequently decay and that increasing ϕ_b provides a delayed and enhanced peak. These findings are consistent with the observations made with the predictions of the modified Benney equation (see Sec. IV A). The inset in Fig. 13(a) shows the initial growth remaining the same for the two Peclet numbers. This is because the linear growth

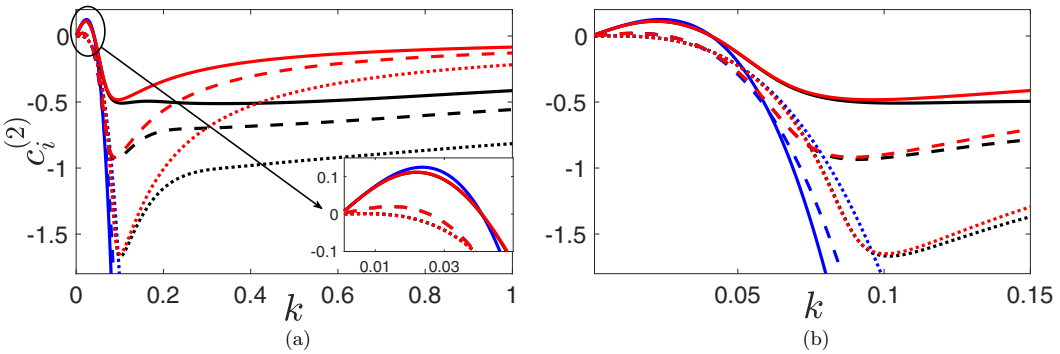

FIG. 12. Comparison of growth rate between linearized Benney equations (blue lines), linearized IBL equations (red lines) and linear stability analysis (black lines) for the case of Re = 20, (—) $\phi_b = 0.1$, (- - -) $\phi_b = 0.2$, and (· · ·) $\phi_b = 0.3$ with We = 10^3 and $\alpha = 45°$.

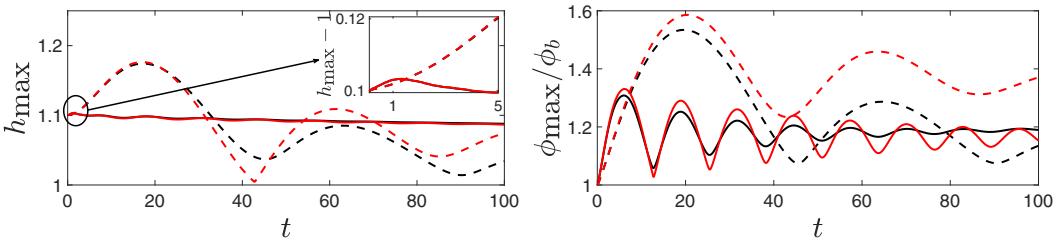

FIG. 13. Evolution of film height h and particle concentration ϕ with Re $= 12$, We $= 10^3$, inclination $\alpha = 45^\circ$, and $k \approx k_c$ for the corresponding initial particle concentrations (—) $\phi_b = 0.01$; (- - -) $\phi_b = 0.1$; Pe $= 1$ (black lines) and Pe $= 2$ (red lines). Inset in (a) shows the initial growth of the height perturbation $h_{\max} - 1$.

rate is independent of the choice of Peclet number [see Eq. (77)]. However, we observe that the oscillatory decay of the height perturbation is slower for the higher value of Peclet number.

The evolution of the free-surface waveforms over time for the previously mentioned cases are visualized in Fig. 14. It is immediately apparent that the higher particle volume fraction slows down the wave due to increased viscosity. To further study this, we plot the wave profiles and streamlines at specific instants of time with disturbance wave numbers $k_s \approx k_c/2$ (taken to be $k = 0.13$ and 0.1 for $\phi_b = 0.01$ and 0.1, respectively) in Fig. 15. We choose smaller wave numbers to study the free-surface waveforms because smaller wave numbers are known to create more noticeable distortions on the wave structure [59]. For $\phi_b = 0.01$, Fig. 15(a) corresponds to the time close to which the initial maximum amplitude of the perturbation is reached. This initial maximum is followed by the formation of secondary waves as indicated in Fig. 15(b). However, although we find that a higher peak is achieved with $\phi_b = 0.1$, no such surface distortions with the incidence of secondary waves can be observed as shown in Figs. 15(c) and 15(d). Further, using the expression for the particle volume fraction field obtained using the central manifold approach [see Eq. (54)], we visualize the particle volume fraction field using a contour plot in Fig. 15. As expected, there is minimal variation in the particle volume fraction field across the depth of the film. We also find that the maximum particle volume fraction occurs at the location where the height of the film is maximum.

V. DISCUSSION

We considered the problem of a colloidal film falling down an incline under the influence of gravity. An advection-diffusion equation dictates the evolution of particles, with the diffusive processes being purely thermal in origin. This is valid under the assumption that the particles are colloidal. A similar advection-diffusion equation, albeit also including the electrostatic contribution to the osmotic pressure, was used to model paint drying by Goehring *et al.* [45], whose predictions provided good agreement with experiments when the suspended particles are of radii $5 - 14$nm. Also, Sobac *et al.* [47] was able to predict the onset of Benard-Marangoni instability correctly for a drying film laden with particles of radii $\approx$12.5nm. The effect of the dispersed phase enters the fluid momentum equation through a particle volume fraction dependent viscosity. Linear stability analysis of the corresponding Orr-Sommerfeld system revealed the presence of two unstable modes, the surface and the shear modes, and a purely damped particle mode. Expectedly, the surface and shear modes are stabilized with increasing particle bulk volume fractions. At leading order, Brownian diffusion dominates and equilibrates the particle volume fraction along the gradient direction. Thus, the film has an increased viscosity throughout the film, leading to a stabilizing effect on the system. The particle mode is a purely damped mode. Nevertheless, it exhibits interesting dynamics based on the magnitude of kPe—the ratio of two timescales, the equilibration time due to molecular diffusion in the gradient direction (h_0^2/D), and the convective timescale associated with

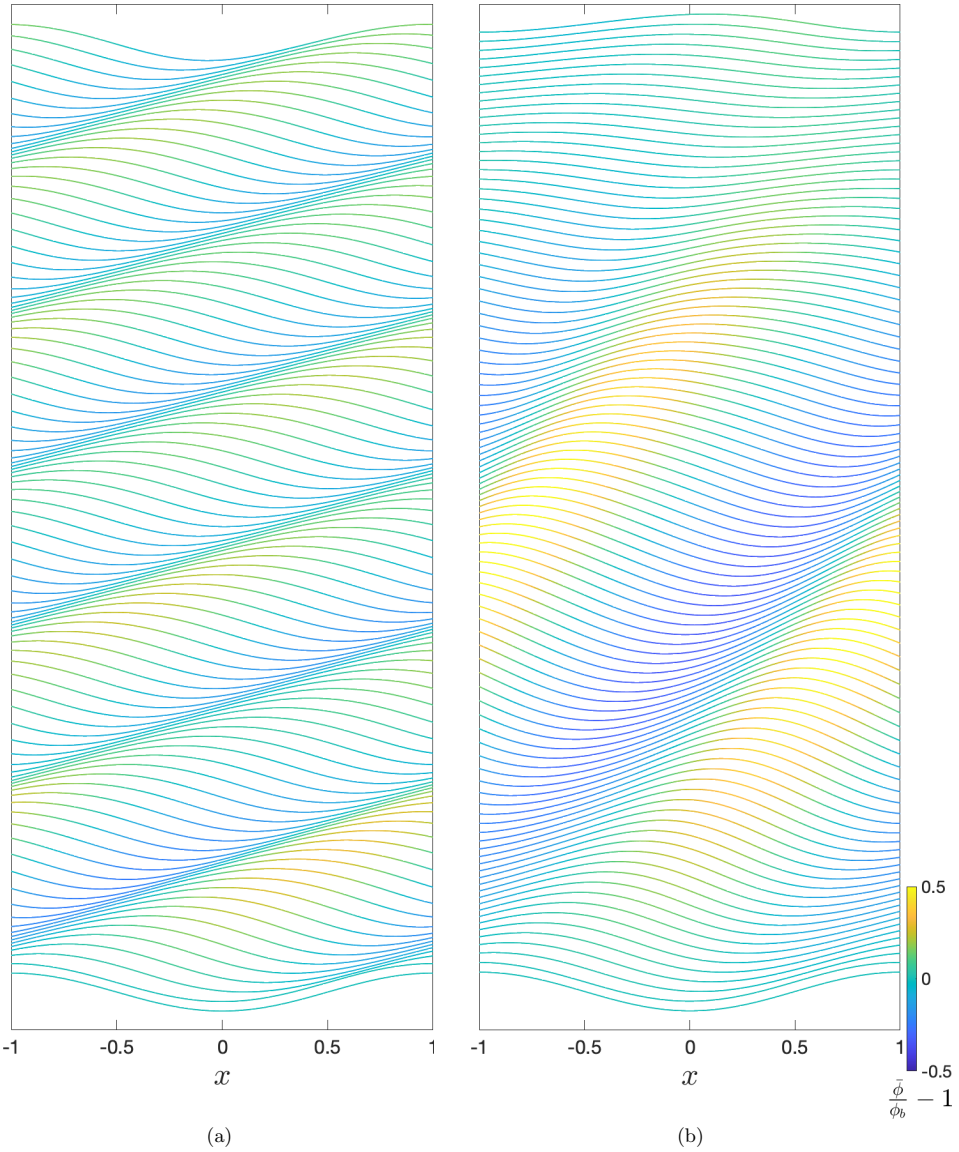

FIG. 14. Free-surface wave forms with $k \approx k_c$ for two particle volume fractions with the time interval between two waves being 5 with Re $= 12$, Pe $= 1$, We $= 10^3$, and inclination $\alpha = 45^\circ$. (a) $\phi_b = 0.01$ and (a) $\phi_b = 0.1$.

streamwise transport over a disturbance wavelength (λ/U_0). The decay rate of the particle mode thus has three asymptotic states: a Brownian mode, a Taylor mode, and an anomalous mode.

The linear stability analysis with the Orr-Sommerfeld equations hinges on the assumption that the amplitude of disturbances is infinitesimal. To study the formation and evolution of nonlinear waves in a colloidal falling film, we next derived a system of depth-averaged equations under the long-wave approximation. In earlier studies, the depth-averaged dynamics of the particulate phase has been described by a transport equation that includes advection by the fluid and streamwise molecular diffusion. However, in the context of solute transport in channels, Taylor [57] showed that there could be an enhanced dispersion of solutes along the flow direction, aided by shear. This shear-enhanced

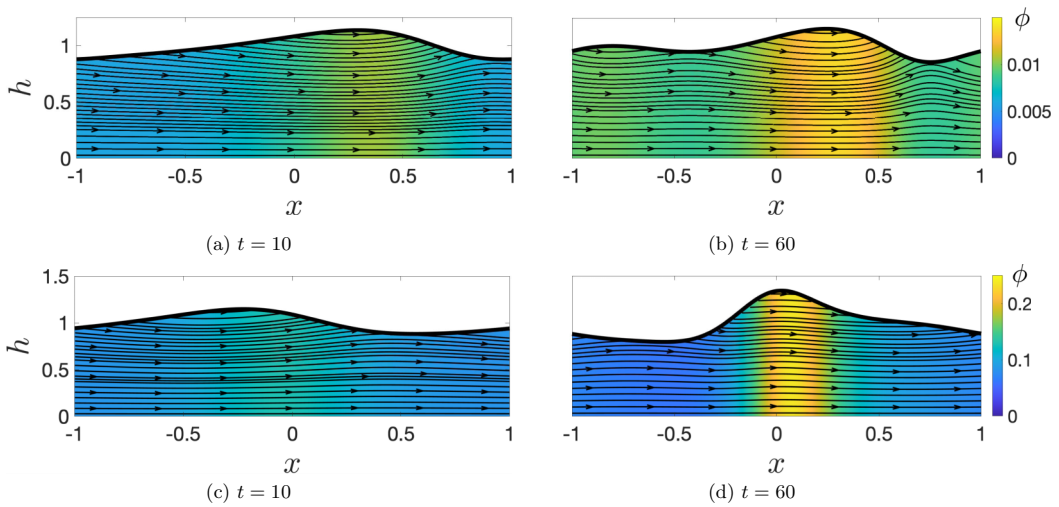

FIG. 15. Wave profiles and streamlines at different instants in time for the corresponding initial particle concentrations (a), (b) $\phi_b = 0.01$; (c), (d) $\phi_b = 0.1$; (c), (d) excited with wave numbers $k \approx k_s$. Re $= 12$, Pe $= 1$, We $= 10^3$, and inclination $\alpha = 45^\circ$. The contour plot shows the particle volume fraction field.

dispersion, eponymously known as Taylor dispersion, has previously been calculated in the context of particle-laden flow inside a pressure-driven pipe flow [69,70] and a gravity-driven dense granular flow [71]. It has also been studied in the context of the dispersion of a solute in a channel with periodically varying apertures [72]. Ramachandran [70] used a multiple-timescale expansion technique to arrive at a nonlinear equation for the flow of a noncolloidal suspension ($\mathrm{Pe}_p \gg 1$) inside a pipe with the absence of fluid inertia (Re $= 0$). We followed a center-manifold-based approach for the depth-averaged particle volume fraction equation to incorporate Taylor dispersion in this work. Our choice of approach was due to the necessity of obtaining an explicit expression for the particle concentration field valid till $\mathcal{O}(\epsilon)$ since it is required to close the system of equations and to capture the effects of Taylor dispersion. The novelty in our calculation lies in integrating the physics of shear-enhanced dispersion with a nonlinearly evolving free boundary.

The description of the particle concentration is incomplete without the knowledge of the film height and flux. To model the evolution of the film height, we initially derived a Benney-type evolution equation. This long-wave approximation assumes that the variations in the disturbance occur over long wavelengths but does not restrict the disturbance amplitude. Numerical solutions of the modified Benney equations revealed an intriguing feature—although the presence of particles reduced the growth rates, the film height reached a delayed and enhanced peak for increasing particle concentrations. We found this to be a consequence of the nonlinear dynamics of the two-way coupled system since we did not see an enhanced peak for higher particle concentrations with the corresponding one-way coupled system.

Benney-type nonlinear equations are ideal for studying the nonlinear regime, provided we restrict ourselves to the near-Stokesian regime, studying the effects of small fluid inertia. However, these equations are susceptible to finite time blowups when the effects of fluid inertia are strong [17]. To address this, we derived an IBL model using a weighted residuals based approach formulated by Ruyer-Quil and Manneville [67]. As mentioned previously, the Orr-Sommerfeld equation assumes that the disturbance amplitudes are small. In contrast, the long-wave approximation of the two model equations assumes that variations happen over long wavelengths. This implies that the predictions of the three systems should be consistent in the small-amplitude and small wave-number limit. To check this, we performed a linear stability analysis on the model equations and compared the predictions across the three systems of equations. We found that modified Benney equations were

consistent with the Orr-Sommerfeld equations for a narrow range of small wave numbers. The IBL equations' predictions were consistent with the Orr-Sommerfeld equations in the limit of small wave numbers, albeit for a more extensive range. The numerical simulations of the nonlinear system revealed trends similar to those observed with the modified Benney equations. Plotting the free-surface waveforms, we found that increasing particle volume fractions leads to both the retardation of flow and the suppression of surface deformations. It must be noted that as derived by Roberts [73], it is possible to obtain the equation for the film height using a central manifold approach as done here for the particle concentration field. However, as later pointed out by Ruyer-Quil [74], the central manifold approach brings out a system that is nearly identical to the one obtained using the IBL approach, albeit with slightly different coefficients, when restricted to $\mathcal{O}(\epsilon)$ accuracy. At orders higher than $\mathcal{O}(\epsilon)$, the two approaches provide different results. This is because of the restriction $\epsilon\mathrm{Re} = \mathcal{O}(1)$ for the central manifold approach to be valid, whereas IBL places no such restriction. Therefore, we chose to take the IBL approach for the momentum equation.

An important caveat in this study is the exclusion of the effect of particle concentration on altering the interfacial properties—surface tension and surface viscosity. We incorporate only the depth-averaged particle volume fraction ($\bar{\phi}$) in the nonlinear models. However, one would note that the local particle volume fraction at the interface is equal to $\bar{\phi}$ at leading order due to the dominance of diffusion in gradient direction [see Eq. (54)]. Thus our reduced order model will insufficiently capture the interfacial dynamics of concentrated systems. When the free interface becomes particle rich such that it approaches a jammed state, the interface could behave like an elastic solid [75]. The free interface with a jammed monolayer of floating particles will behave like a flexible sheet that can undergo buckling instability under compression [76], while also altering the surface tension [77]. Suppose we were to extend our calculations to higher particle volume fractions. In that case, our model needs to be augmented with concentration-dependent surface tension and surface viscosity [78] which would possibly introduce the additional physics of Marangoni effects.

This paper has focused on free surface flows laden with neutrally buoyant particles that are small enough that Brownian diffusion dominates. Therefore, we ignore the roles of shear-induced migration and particle-induced normal stresses on the system [54]. Shear-induced migration could lead to particle accumulation at the free interface, resulting in a nonuniform viscosity profile in the base state. Viscosity stratification, due to thermal effects, is known to influence the stability characteristics of falling film flows [79]. In a separate study, we studied the linear stability of a particle-laden shallow flow with the inclusion of shear-induced migration [80]. There, we modeled the particle flux as one that flows due to the divergence of the particle induced normal stresses as [81]

$$\boldsymbol{J} = \tfrac{2}{9} f(\phi) \boldsymbol{\nabla} \cdot \boldsymbol{\Sigma}^p, \tag{78}$$

$$\boldsymbol{\Sigma}^p = \boldsymbol{\Sigma}^{\mathrm{NS}} + (\mu(\phi) - \mu_f)(\boldsymbol{\nabla u} + \boldsymbol{\nabla u}^T), \tag{79}$$

Since we were interested in the regime of finite Pe_p, meaning the particles' contribution to both the thermal and hydrodynamic contributions are together present, we wrote the particle-induced normal stresses without loss of generality as

$$\boldsymbol{\Sigma}^{\mathrm{NS}}_{\alpha\alpha} = -\left[\frac{9}{2}\frac{1}{\mathrm{Pe}_p}\mathcal{A} + \mathcal{Q}_{\alpha\alpha}\right], \tag{80}$$

where $\alpha = x, y$ or z. Here $\mathcal{A}$ denotes the isotropic thermal contribution to the particle induced normal stresses—one that is dominant at $\mathrm{Pe}_p \ll 1$, whereas $\mathcal{Q}_{\alpha\alpha}$ denotes the anisotropic hydrodynamic contribution. We subsequently used the model by Buyevich and Kapbsov [82] for $\mathcal{A}$ and the model by Frank *et al.* [83] for $\mathcal{Q}_{\alpha\alpha}$. We found that with particles whose Peclet number (Pe_p) is $\mathcal{O}(1)$, the effects of base-state viscosity stratification and momentum forcing arising from the particle concentration perturbation, both being consequences of shear-induced migration, lead to an enhanced destabilization of both the surface and shear modes of instability.

VI. SUMMARY

We have investigated the linear stability of a particle-laden, gravity-driven, shallow free-surface flow down an incline and the subsequent formation of nonlinear waves. The particles considered were neutrally buoyant and colloidal. We first performed a linear stability analysis and identified the particles' stabilizing effect on both the surface and shear modes of instability. Based on the magnitude of kPe, the damped particle mode decays via three asymptotic states: Brownian diffusion, anomalous diffusion, and Taylor dispersion. Next, we use the insights gained from the linear stability to formulate nonlinear reduced-order models. To incorporate Taylor dispersion along with Brownian diffusion, we use a central manifold approach to derive the depth-averaged particle volume fraction. For the film height, we derived nonlinear models in the framework of long-wave theory using Benney's gradient expansion approach and the IBL approach.

The current paper incorporating the role of Brownian diffusion solely and its stabilizing effect aims to act as a step toward developing nonlinear reduced-order models for shallow particle-laden flows. Extending this, a reduced-order nonlinear model that would include the physics of normal stresses, shear-induced migration, particle inertia, and buoyancy effects in the dispersed phase will be beneficial in studying various free surface problems involving sediment transport [84].

APPENDIX A: NUMERICAL METHOD FOR SOLVING THE LINEAR STABILITY EQUATIONS

Equations (20) and (21) are solved numerically for the eigenvalue c using a spectral collocation method. For this, we first use Lagrange polynomials to approximate the solution of $\hat{\psi}$ and $\hat{\phi}$, and discretize the physical domain using Chebyshev grid points [61]:

$$\hat{\psi} = \sum_{j=0}^{N-1} L_{ij}\hat{\psi}_j, \qquad \hat{\phi} = \sum_{j=0}^{N-1} L_{ij}\hat{\phi}_j, \qquad c = \sum_{j=0}^{N-1} L_{ij}c_j. \tag{A1}$$

Here, $\hat{\psi}_j$, $\hat{\phi}_j$, and c_j are $\hat{\psi}$, $\hat{\phi}$, and c at Chebyshev grid points $z_j = \cos(j\pi/N)$, and N is the number of collocation points used to discretize the domain. The Chebyshev grid points lie in the interval $[-1,1]$, whereas the physical domain of the problem lies in the interval $[0,1]$. Therefore, we map the Chebyshev grid points to the domain $[0,1]$ using the relation $y_j = 0.5(1 - z_j)$. The boundary condition given in Eq. (23) is nonlinear in the eigenvalue c. To avoid this nonlinearity, we use the kinematic boundary condition and write an additional equation for the scalar height field h as

$$\{\kappa_b(\mathcal{D}^2 - 3k^2)\mathcal{D} + ik\mathrm{Re}(c - u_b(1))\mathcal{D}\}\hat{\psi} - ik(3\cot\theta + k^2\ \mathrm{We}\ \mathrm{Re})h + \kappa_{b1}\mathcal{D}(u_b'\hat{\phi}) = 0, \tag{A2}$$

$$ch = \psi + u_b(1)h. \tag{A3}$$

The resulting system can be written in the form of a generalized eigenvalue problem as

$$\mathbf{A}\cdot\mathbf{q} = c\,\mathbf{B}\cdot\mathbf{q}, \tag{A4}$$

where, $\mathbf{q} = \{\hat{\psi}_j, \hat{\phi}_j, h\}$, and $\mathbf{A}$ and $\mathbf{B}$ are matrices of the order $2N + 3$. We then proceed to solve the above eigenvalue problem using the MATLAB subroutine eig.

APPENDIX B: TAYLOR DISPERSION—DERIVATION OF V^n AND G^n

At $n = 0$,

$$\Upsilon\frac{\partial^2 V^0}{\partial y^2} = 0, \tag{B1}$$

with boundary conditions at $y = 0$ and $y = 1$ as

$$\Upsilon\frac{\partial V^0}{\partial y} = 0. \tag{B2}$$

Solving the above system, we obtain

$$V^0 = \bar{\phi}(x,t), \tag{B3}$$

where $\bar{\phi}(x,t)$ denotes the depth-averaged particle volume fraction. Subsequently, at $n = 1$ we have

$$\Upsilon \frac{\partial^2 V^1}{\partial y^2} = \mathrm{Pe}\left(G^1 + u\frac{\partial \bar{\phi}}{\partial x} \right), \tag{B4}$$

with boundary conditions at $y = 0$ and $y = 1$ as

$$\Upsilon \frac{\partial V^1}{\partial y} = 0. \tag{B5}$$

Integrating the above system from $y = 0$ to h and applying the boundary conditions, we obtain

$$G^1 = -\frac{q}{h}\frac{\partial \bar{\phi}}{\partial x}. \tag{B6}$$

Thus the equation at $n = 1$ becomes

$$\Upsilon \frac{\partial^2 V^1}{\partial y^2} = \mathrm{Pe}\left(-\frac{q}{h}\frac{\partial \bar{\phi}}{\partial x} + u\frac{\partial \bar{\phi}}{\partial x} \right). \tag{B7}$$

To calculate V^1, we integrate the above equation twice with respect to y to obtain

$$\Upsilon V^1 = \mathrm{Pe}\left[-\frac{y}{2}\frac{q}{h}\frac{\partial \bar{\phi}}{\partial x} + \frac{qh}{2}\left(\bar{y}^3 - \frac{\bar{y}^4}{4} \right)\frac{\partial \bar{\phi}}{\partial x} \right] + a_1 y + a_2. \tag{B8}$$

Using the boundary condition at $y = 0$, $a_1 = 0$. With the boundary condition at $y = 1$, we obtain

$$a_2 = \mathrm{Pe}\frac{qh}{15}\frac{\partial \bar{\phi}}{\partial x}. \tag{B9}$$

Thus,

$$V^1 = \frac{\mathrm{Pe}}{\Upsilon} qh\left(-\frac{\bar{y}^2}{2} + \frac{\bar{y}^3}{2} - \frac{\bar{y}^4}{8} + \frac{1}{15} \right)\frac{\partial \bar{\phi}}{\partial x}. \tag{B10}$$

Finally, to evaluate G^2 and V^2, we write the $n = 2$ equation as

$$\Upsilon \frac{\partial^2 V^2}{\partial y^2} = \mathrm{Pe}\left[\frac{\partial V^1}{\partial t} + V^0_{\bar{\phi}} G^2 + V^1_{\bar{\phi}} G^1 + V^1_{\bar{\phi}'}\frac{\partial G^1}{\partial x} + u\frac{\partial V^1}{\partial x} + v\frac{\partial V^1}{\partial y} \right] - \frac{\partial}{\partial x}\left(\Upsilon \frac{\partial V^0}{\partial x} \right). \tag{B11}$$

Here, $\bar{\phi}' = \partial\bar{\phi}/\partial x$, $V^0_{\bar{\phi}} = \partial V^0/\partial\bar{\phi}$, $V^1_{\bar{\phi}} = \partial V^1/\partial\bar{\phi}$, and $V^1_{\bar{\phi}} = \partial V^1/\partial\bar{\phi}'$. This is complemented with boundary conditions at $y = 0$,

$$\Upsilon \frac{\partial V^2}{\partial y} = 0, \tag{B12}$$

and at $y = 1$:

$$\Upsilon \frac{\partial V^2}{\partial y} = \Upsilon \frac{\partial h}{\partial x}\frac{\partial V^0}{\partial x}. \tag{B13}$$

As with the case of $n = 1$, we integrate the above system from $y = 0$ to h and use the boundary conditions to obtain

$$G^2 = \frac{1}{\mathrm{Pe}}\frac{\partial}{\partial x}\left(\Upsilon\frac{\partial\bar{\phi}}{\partial x}\right) + \frac{\Upsilon}{\mathrm{Pe}}\frac{\partial h}{\partial x}\frac{\partial\bar{\phi}}{\partial x} + \frac{\mathrm{Pe}}{\Upsilon}\left(\frac{2}{105}q^2\frac{\partial^2\bar{\phi}}{\partial x^2} + \frac{2}{105}\frac{q^2}{h}\frac{\partial\bar{\phi}}{\partial x}\frac{\partial h}{\partial x}\right.$$
$$\left. - \frac{2}{105}q^2\frac{\Upsilon_{\bar{\phi}}}{\Upsilon}\left(\frac{\partial\bar{\phi}}{\partial x}\right)^2 + \frac{4}{105}q\frac{\partial\bar{\phi}}{\partial x}\frac{\partial q}{\partial x}\right). \tag{B14}$$

Substituting G^2 in Eq. (B11), integrating twice with respect to y and using the boundary conditions, we obtain V^2 as

$$V^2 = h\left(\frac{\bar{y}^2}{2} - \frac{1}{6}\right)\frac{\partial h}{\partial x}\frac{\partial\bar{\phi}}{\partial x} + h^2 q\frac{\mathrm{Pe}^2}{\Upsilon(\bar{\phi})^2}\left(-\frac{1}{315} + \frac{\bar{y}^2}{240} + \frac{\bar{y}^4}{24} - \frac{\bar{y}^5}{20} + \frac{\bar{y}^6}{80}\right)\frac{\partial h}{\partial t}\frac{\partial\bar{\phi}}{\partial x}$$
$$+ h^3\frac{\mathrm{Pe}^2}{\Upsilon(\bar{\phi})^2}\left(-\frac{2}{315} + \frac{\bar{y}^2}{30} - \frac{\bar{y}^4}{24} + \frac{\bar{y}^5}{40} - \frac{\bar{y}^6}{240}\right)\frac{\partial q}{\partial t}\frac{\partial\bar{\phi}}{\partial x}$$
$$+ hq^2\frac{\mathrm{Pe}^2}{\Upsilon(\bar{\phi})^2}\left(-\frac{4}{225} + \frac{8\bar{y}^2}{105} + \frac{\bar{y}^3}{30} - \frac{11\bar{y}^4}{120} - \frac{\bar{y}^5}{40} + \frac{\bar{y}^6}{15} - \frac{3\bar{y}^7}{112} + \frac{3\bar{y}^8}{896}\right)\frac{\partial h}{\partial x}\frac{\partial\bar{\phi}}{\partial x}$$
$$+ h^2 q\frac{\mathrm{Pe}^2}{\Upsilon(\bar{\phi})^2}\left(\frac{17}{1575} - \frac{43\bar{y}^2}{560} + \frac{\bar{y}^3}{30} + \frac{3\bar{y}^4}{40} - \frac{\bar{y}^5}{20} - \frac{\bar{y}^6}{120} + \frac{\bar{y}^7}{112} - \frac{\bar{y}^8}{896}\right)\frac{\partial q}{\partial x}\frac{\partial\bar{\phi}}{\partial x}$$
$$+ h^2(1-\mathrm{Pe})\left(\frac{1}{6} - \frac{\bar{y}^2}{2}\right)\frac{\partial^2\bar{\phi}}{\partial x^2} + q^2h^2\frac{\mathrm{Pe}^2}{\Upsilon(\bar{\phi})^2}\left(\frac{4}{525} - \frac{2\bar{y}^2}{35} + \frac{\bar{y}^3}{30} + \frac{3\bar{y}^4}{40}\right.$$
$$\left. - \frac{\bar{y}^5}{8} + \frac{\bar{y}^6}{12} - \frac{3\bar{y}^7}{112} + \frac{3\bar{y}^8}{896}\right)\frac{\partial^2\bar{\phi}}{\partial x^2} + h^2\frac{\Upsilon(\bar{\phi})_{\bar{\phi}}}{\Upsilon(\bar{\phi})}(1-\mathrm{Pe})\left(\frac{1}{6} - \frac{\bar{y}^2}{2}\right)\left(\frac{\partial\bar{\phi}}{\partial x}\right)^2$$
$$+ q^2h^2\frac{\mathrm{Pe}^2\Upsilon(\bar{\phi})_{\bar{\phi}}}{\Upsilon(\bar{\phi})^3}\left(-\frac{2}{1575} + \frac{\bar{y}^2}{42} - \frac{\bar{y}^3}{30} - \frac{\bar{y}^4}{30} + \frac{\bar{y}^5}{10} - \frac{19\bar{y}^6}{240} + \frac{3\bar{y}^7}{112} - \frac{3\bar{y}^8}{896}\right)\left(\frac{\partial\bar{\phi}}{\partial x}\right)^2. \tag{B15}$$

[1] P. L. Kapitza and S. Kapitza, Wave flow of thin layers of viscous liquids. Part III. Experimental research of a wave flow regime, Zh. Eksp. Teor. Fiz. **19**, 105 (1949).

[2] R. Verma, A. Sharma, K. Kargupta, and J. Bhaumik, Electric field induced instability and pattern formation in thin liquid films, Langmuir **21**, 3710 (2005).

[3] J. Pascal, S. D'Alessio, and M. Hasan, Instability of gravity-driven flow of a heated power-law fluid with temperature dependent consistency, AIP Adv. **8**, 105215 (2018).

[4] T. P. Witelski and A. J. Bernoff, Stability of self-similar solutions for van der Waals driven thin film rupture, Phys. Fluids **11**, 2443 (1999).

[5] P. Gaskell, P. Jimack, M. Sellier, H. Thompson, and M. Wilson, Gravity-driven flow of continuous thin liquid films on non-porous substrates with topography, J. Fluid Mech. **509**, 253 (1999).

[6] A. De Wit, D. Gallez, and C. Christov, Nonlinear evolution equations for thin liquid films with insoluble surfactants, Phys. Fluids **6**, 3256 (1994).

[7] A. Oron, S. H. Davis, and S. G. Bankoff, Long-scale evolution of thin liquid films, Rev. Mod. Phys. **69**, 931 (1997).

[8] R. V. Craster and O. K. Matar, Dynamics and stability of thin liquid films, Rev. Mod. Phys. **81**, 1131 (2009).

[9] S. Kalliadasis, C. Ruyer-Quil, B. Scheid, and M. G. Velarde, *Falling Liquid Films*, Applied Mathematical Sciences Vol. 176 (Springer Science & Business Media, New York, 2011).

[10] T. B. Benjamin, Wave formation in laminar flow down an inclined plane, J. Fluid Mech. **2**, 554 (1957).
[11] C.-S. Yih, Stability of liquid flow down an inclined plane, Phys. Fluids **6**, 321 (1963).
[12] M. K. Smith, The mechanism for the long-wave instability in thin liquid films, J. Fluid Mech. **217**, 469 (1990).
[13] P. J. Schmid and D. S. Henningson, *Stability and Transition in Shear Flows* (Springer, New York, NY, 2001).
[14] R. Chin, F. Abernath, and J. Bertschy, Gravity and shear wave stability of free surface flows. Part 1. Numerical calculations, J. Fluid Mech. **168**, 501 (1986).
[15] J. Floryan, S. Davis, and R. Kelly, Instabilities of a liquid film flowing down a slightly inclined plane, Phys. Fluids **30**, 983 (1987).
[16] D. Benney, Long waves on liquid films, J. Math. Phys. **45**, 150 (1966).
[17] A. Pumir, P. Manneville, and Y. Pomeau, On solitary waves running down an inclined plane, J. Fluid Mech. **135**, 27 (1983).
[18] G. Homsy, Model equations for wavy viscous film flow, Lect. Appl. Math. **15**, 19 (1974).
[19] J. M. Hyman, B. Nicolaenko, and S. Zaleski, Order and complexity in the Kuramoto-Sivashinsky model of weakly turbulent interfaces, Physica D **23**, 265 (1986).
[20] A. Oron and O. Gottlieb, Nonlinear dynamics of temporally excited falling liquid films, Phys. Fluids **14**, 2622 (2002).
[21] V. Y. Shkadov, Wave flow regimes of a thin layer of viscous fluid subject to gravity, Fluid Dyn. **2**, 29 (1970).
[22] S. Kalliadasis, E. Demekhin, C. Ruyer-Quil, and M. Velarde, Thermocapillary instability and wave formation on a film falling down a uniformly heated plane, J. Fluid Mech. **492**, 303 (2003).
[23] S. Kalliadasis, A. Kiyashko, and E. Demekhin, Marangoni instability of a thin liquid film heated from below by a local heat source, J. Fluid Mech. **475**, 377 (2003).
[24] C. Ruyer-Quil, B. Scheid, S. Kalliadasis, M. G. Velarde, and R. K. Zeytounian, Thermocapillary long waves in a liquid film flow. Part 1. Low-dimensional formulation, J. Fluid Mech. **538**, 199 (2005).
[25] B. Scheid, C. Ruyer-Quil, S. Kalliadasis, M. G. Velarde, and R. K. Zeytounian, Thermocapillary long waves in a liquid film flow. Part 2. Linear stability and nonlinear waves, J. Fluid Mech. **538**, 223 (2005).
[26] P. Trevelyan, B. Scheid, C. Ruyer-Quil, and S. Kalliadasis, Heated falling films, J. Fluid Mech. **592**, 295 (2007).
[27] O. Pouliquen, On the shape of granular fronts down rough inclined planes, Phys. Fluids **11**, 1956 (1999).
[28] J. Gray and A. Edwards, A depth-averaged-rheology for shallow granular free-surface flows, J. Fluid Mech. **755**, 503 (2014).
[29] V. Kumaran, Dense shallow granular flows, J. Fluid Mech. **756**, 555 (2014).
[30] J. Baker, C. Johnson, and J. Gray, Segregation-induced finger formation in granular free-surface flows, J. Fluid Mech. **809**, 168 (2016).
[31] W. B. Russel, D. A. Saville, and W. R. Schowalter, *Colloidal Dispersions*, Cambridge Monographs on Mechanics (Cambridge University Press, Cambridge, 1989).
[32] A. Einstein, A new determination of molecular dimensions, Ann. Phys. **324**, 289 (1906).
[33] G. K. Batchelor and J. T. Green, The hydrodynamic interaction of two small freely-moving spheres in a linear flow field, J. Fluid Mech. **56**, 375 (1972).
[34] R. J. Phillips, R. C. Armstrong, R. A. Brown, A. L. Graham, and J. R. Abbott, A constitutive equation for concentrated suspensions that accounts for shear-induced particle migration, Phys. Fluids **4**, 30 (1992).
[35] D. Merhi, E. Lemaire, G. Bossis, and F. Moukalled, Particle migration in a concentrated suspension flowing between rotating parallel plates: Investigation of diffusion flux coefficients, J. Rheol. **49**, 1429 (2005).
[36] N. Murisic, B. Pausader, D. Peschka, and A. L. Bertozzi, Dynamics of particle settling and resuspension in viscous liquid films, J. Fluid Mech. **717**, 203 (2013).
[37] Leonardo Espín and S. Kumar, Forced spreading of films and droplets of colloidal suspensions, J. Fluid Mech. **742**, 495 (2014).

[38] B. P. Cook, A theory for particle settling and shear-induced migration in thin film flow, Phys. Rev. E **78**, 045303(R) (2008).
[39] N. Murisic, J. Ho, V. Hu, P. Latterman, T. Koch, K. Lin, M. Mata, and A. Bertozzi, Particle-laden viscous thin-film flows on an incline: Experiments compared with a theory based on shear-induced migration and particle settling, Physica D **240**, 1661 (2011), Special Issue: Fluid Dynamics: From Theory to Experiment.
[40] H. Schmidt, Nanoparticles by chemical synthesis, processing to materials and innovative applications, Appl. Organometal. Chem. **15**, 331 (2001).
[41] H. Yoo and C. Kim, Experimental studies on formation, spreading and drying of inkjet drop of colloidal suspensions, Colloids Surf., A **468**, 234 (2015).
[42] H. M. van der Kooij and J. Sprakel, Watching paint dry; more exciting than it seems, Soft Matter **11**, 6353 (2015).
[43] W. B. Russel, Mechanics of drying colloidal dispersions: Fluid/solid transitions, skinning, crystallization, cracking, and peeling, AIChE J. **57**, 1378 (2011).
[44] A. F. Routh, Drying of thin colloidal films, Rep. Prog. Phys. **76**, 046603 (2013).
[45] L. Goehring, J. Li, and P.-C. Kiatkirakajorn, Drying paint: From micro-scale dynamics to mechanical instabilities, Philos. Trans. R. Soc. A **375**, 20160161 (2017).
[46] M. Wang and J. F. Brady, Microstructures and mechanics in the colloidal film drying process, Soft Matter **13**, 8156 (2017).
[47] B. Sobac, P. Colinet, and L. Pauchard, Influence of Bénard-Marangoni instability on the morphology of drying colloidal films, Soft Matter **15**, 2381 (2019).
[48] S. S. Peppin, M. G. Worster, and J. Wettlaufer, Morphological instability in freezing colloidal suspensions, Proc. R. Soc. A. **463**, 723 (2007).
[49] J. Zhou, B. Dupuy, A. L. Bertozzi, and A. E. Hosoi, Theory for Shock Dynamics in Particle-Laden Thin Films, Phys. Rev. Lett. **94**, 117803 (2005).
[50] A. Mavromoustaki, L. Wang, J. Wong, and A. Bertozzi, Surface tension effects for particle settling and resuspension in viscous thin films, Nonlinearity **31**, 3151 (2018).
[51] Y. Chen, R. Luo, L. Wang, and S. Lee, Self-similarity in particle accumulation on the advancing meniscus, J. Fluid Mech. **925**, A10 (2021).
[52] T. Pham and S. Kumar, Imbibition and evaporation of droplets of colloidal suspensions on permeable substrates, Phys. Rev. Fluids **4**, 034004 (2019).
[53] G. Mercer and A. Roberts, A centre manifold description of contaminant dispersion in channels with varying flow properties, SIAM J. Appl. Math. **50**, 1547 (1990).
[54] E. Guazzelli and O. Pouliquen, Rheology of dense granular suspensions, J. Fluid Mech. **852**, P1 (2018).
[55] M. Latini and A. J. Bernoff, Transient anomalous diffusion in poiseuille flow, J. Fluid Mech. **441**, 399 (2001).
[56] R. Camassa, R. M. McLaughlin, and C. Viotti, Analysis of passive scalar advection in parallel shear flows: Sorting of modes at intermediate time scales, Phys. Fluids **22**, 117103 (2010).
[57] G. I. Taylor, Dispersion of soluble matter in solvent flowing slowly through a tube, Proc. R. Soc. London A **219**, 186 (1953).
[58] P. Haynes and J. Vanneste, Dispersion in the large-deviation regime. Part 2. Cellular flow at large Péclet number, J. Fluid Mech. **745**, 351 (2014).
[59] S. Miladinova, G. Lebon, and E. Toshev, Thin-film flow of a power-law liquid falling down an inclined plate, J. Non-Newtonian Fluid Mech. **122**, 69 (2004).
[60] J. Pascal, Linear stability of fluid flow down a porous inclined plane, J. Phys. D **32**, 417 (1999).
[61] L. N. Trefethen, *Spectral Methods in MATLAB* (SIAM, Philadelphia, 2000).
[62] P. G. Drazin and W. H. Reid, *Hydrodynamic Stability* (Cambridge University Press, Cambridge, 2004).
[63] S. A. Maslowe, Critical layers in shear flows, Annu. Rev. Fluid Mech. **18**, 405 (1986).
[64] A. Roberts, The application of centre-manifold theory to the evolution of system which vary slowly in space, ANZIAM J. **29**, 480 (1988).
[65] W. a. Young and S. Jones, Shear dispersion, Phys. Fluids **3**, 1087 (1991).
[66] I. M. R. Sadiq and R. Usha, Thin newtonian film flow down a porous inclined plane: Stability analysis, Phys. Fluids **20**, 022105 (2008).

[67] C. Ruyer-Quil and P. Manneville, Improved modeling of flows down inclined planes, Eur. Phys. J. B **15**, 357 (2000).
[68] A. Samanta, C. Ruyer-Quil, and B. Goyeau, A falling film down a slippery inclined plane, J. Fluid Mech. **684**, 353 (2011).
[69] I. Griffiths and H. A. Stone, Axial dispersion via shear-enhanced diffusion in colloidal suspensions, Europhys. Lett. **97**, 58005 (2012).
[70] A. Ramachandran, A macrotransport equation for the particle distribution in the flow of a concentrated, non-colloidal suspension through a circular tube, J. Fluid Mech. **734**, 219 (2013).
[71] I. C. Christov and H. A. Stone, Shear dispersion in dense granular flows, Granular Matter **16**, 509 (2014).
[72] D. Bolster, M. Dentz, and T. Le Borgne, Solute dispersion in channels with periodically varying apertures, Phys. Fluids **21**, 056601 (2009).
[73] A. Roberts, Low-dimensional models of thin film fluid dynamics, Phys. Lett. A **212**, 63 (1996).
[74] C. Ruyer-Quil, Instabilities and modeling of falling film flows, Ph.D. thesis, Université Pierre et Marie Curie-Paris VI, 2012.
[75] H. N. Dixit and G. Homsy, The elastic Landau-Levich problem, J. Fluid Mech. **732**, 5 (2013).
[76] D. Vella, P. Aussillous, and L. Mahadevan, Elasticity of an interfacial particle raft, Europhys. Lett. **68**, 212 (2004).
[77] H. N. Dixit and G. Homsy, The elastocapillary Landau–Levich problem, J. Fluid Mech. **735**, 1 (2013).
[78] T. Hu, Q. Fu, and L. Yang, Falling film with insoluble surfactants: Effects of surface elasticity and surface viscosities, J. Fluid Mech. **889**, A16 (2020).
[79] D. Goussis and R. E. Kelly, Effects of viscosity variation on the stability of film flow down heated or cooled inclined surfaces: Long-wavelength analysis, Phys. Fluids **28**, 3207 (1985).
[80] D. J. Dhas and A. Roy, Stability of gravity-driven particle-laden flows: Roles of shear-induced migration and normal stresses, J. Fluid Mech. **938**, A29 (2022).
[81] J. F. Morris and F. Boulay, Curvilinear flows of noncolloidal suspensions: The role of normal stresses, J. Rheol. **43**, 1213 (1999).
[82] Y. A. Buyevich and S. Kapbsov, Segregation of a fine suspension in channel flow, J. Non-Newtonian Fluid Mech. **86**, 157 (1999).
[83] M. Frank, D. Anderson, E. R. Weeks, and J. F. Morris, Particle migration in pressure-driven flow of a Brownian suspension, J. Fluid Mech. **493**, 363 (2003).
[84] E. Meiburg and B. Kneller, Turbidity currents and their deposits, Annu. Rev. Fluid Mech. **42**, 135 (2010).